Copy 136
RM L53G29

NACA RM L53G29

7453

NACA

RESEARCH MEMORANDUM

A FLIGHT INVESTIGATION AT MACH NUMBERS FROM 0.67 TO

1.81 OF THE LONGITUDINAL STABILITY AND CONTROL

CHARACTERISTICS OF A 60° DELTA-WING MISSILE

CONFIGURATION HAVING AN ALL-MOVABLE TAIL

By Martin T. Moul and Hal T. Baber, Jr.

Langley Aeronautical Laboratory
Langley Field, Va.

NATIONAL ADVISORY COMMITTEE
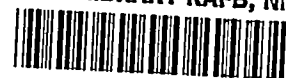# FOR AERONAUTICS
WASHINGTON
October 6, 1953

NATIONAL ADVISORY COMMITTEE FOR AERONAUTICS

RESEARCH MEMORANDUM

A FLIGHT INVESTIGATION AT MACH NUMBERS FROM 0.67 TO

1.81 OF THE LONGITUDINAL STABILITY AND CONTROL

CHARACTERISTICS OF A 60° DELTA-WING MISSILE

CONFIGURATION HAVING AN ALL-MOVABLE TAIL

By Martin T. Moul and Hal T. Baber, Jr.

SUMMARY

In order to determine whether a small, all-movable tail is an effective longitudinal control for a cruciform, delta-wing missile, a flight investigation has been made at Mach numbers from 0.67 to 1.81. Stability, control, hinge-moment, and drag characteristics are presented.

Lift- and pitching-moment-curve slopes and the damping-in-pitch derivative were noted to be dependent upon lift. Pitching effectiveness was maintained at all Mach numbers, but the trim lift produced by tail deflection experienced a reduction of 45 percent with increase of Mach number from 0.80 to 1.60. At low angles of attack the variation of hinge-moment coefficient with angle of attack was nearly linear, but at angles of attack greater than 5°, the variation became very nonlinear. Lift-curve slopes were in good agreement with calculated results based upon the deflected, unwarped vortex concept, but the calculated aerodynamic-center location was farther rearward by 9 to 18 percent of the mean aerodynamic chord.

INTRODUCTION

As part of the general research program on missiles, the Langley Pilotless Aircraft Research Division has been flight testing a series of cruciform, delta-wing missiles. Results of longitudinal stability and control investigations of a tailless model having wing-tip controls and of three canard models having different canard-to-wing distances and canard areas are reported in references 1 to 4. To supplement the available information and show that a small tail in a strong downwash field

may be an effective control surface, a missile configuration employing an all-movable tail has been flight tested.

Stability and control, hinge-moment, and drag characteristics are presented for the Mach number range from 0.67 to 1.81. The stability and control characteristics are compared with approximate theories and with the results of a tailless-missile investigation.

SYMBOLS

a_n/g normal-accelerometer reading, g units

a_l/g longitudinal-accelerometer reading, g units

a_t/g transverse-accelerometer reading, g units

b exponential damping constant in e^{-bt}, per sec

c wing chord, ft

$\bar{c}$ wing mean aerodynamic chord, ft

$\bar{c}_t$ tail mean aerodynamic chord, ft

g acceleration due to gravity, ft/sec^2

q dynamic pressure, lb/sq ft

E Young's modulus of elasticity, $lb/in.^2$

H hinge moment, ft-lb

I plane moment of inertia of body cross section, $in.^4$

I_Y moment of inertia about Y-axis, $slug-ft^2$

M Mach number, V/V_c

P period, sec

R Reynolds number, $\rho\bar{V}\bar{c}/\mu$

S_W total wing area in one plane including body intercept, sq ft

S_t exposed tail area, sq ft

V velocity of model, ft/sec

V_c speed of sound in air, ft/sec

W model weight, lb

C_D drag coefficient, $\left(-\dfrac{a_l}{g}\cos\alpha + \dfrac{a_n}{g}\sin\alpha\right)\dfrac{W}{qS_W}$

C_L lift coefficient, $\left(\dfrac{a_n}{g}\cos\alpha + \dfrac{a_l}{g}\sin\alpha\right)\dfrac{W}{qS_W}$

$C_{L_{trim}}$ trim lift coefficient

C_h hinge-moment coefficient, $\dfrac{H}{qS_t\bar{c}_t}$

C_m pitching-moment coefficient,

$$\dfrac{\text{Pitching moment about center of gravity}}{qS_W\bar{c}}$$

α angle of attack, deg

α_{trim} trim angle of attack, deg

$\dot{\alpha}$ $\dfrac{1}{57.3}\dfrac{d\alpha}{dt}$, radians/sec

δ tail deflection, deg

θ pitch angle, radians

$\dot{\theta}$ pitching velocity, radians/sec

$\ddot{\theta}$ pitching acceleration, radians/sec^2

μ coefficient of viscosity, slugs/ft-sec

ρ mass density of air, slugs/cu ft

ω model damped natural frequency, radians/sec

Derivatives:

$$C_{L_\alpha} = \frac{\partial C_L}{\partial \alpha}, \text{ per deg} \qquad C_{m_\alpha} = \frac{\partial C_m}{\partial \alpha}, \text{ per deg}$$

$$C_{h_\alpha} = \frac{\partial C_h}{\partial \alpha}, \text{ per deg} \qquad C_{m_\delta} = \frac{\partial C_m}{\partial \delta}, \text{ per deg}$$

$$C_{h_\delta} = \frac{\partial C_h}{\partial \delta}, \text{ per deg} \qquad C_{m_q} = \frac{\partial C_m}{\partial \frac{\theta \bar{c}}{2V}}, \text{ per radian}$$

$$C_{m_{\dot\alpha}} = \frac{\partial C_m}{\partial \frac{\dot\alpha \bar{c}}{2V}}, \text{ per radian}$$

MODEL AND APPARATUS

Model Description

The model tested had a body consisting of a 7-inch-diameter cylindrical section and nose and tail sections of ogival profile. The overall fuselage fineness ratio was 16.3. Wings and tail surfaces, all of delta plan form, were mounted on the fuselage in an inline cruciform arrangement. Plan- and side-view sketches of the model, which indicate the relative location of the wings and tail surfaces, are shown in figure 1.

The solid magnesium wings, with leading edges swept back 60°, were flat plates with beveled leading and trailing edges and had a thickness ratio of 3 percent at the wing-body juncture. The tail surfaces, which were constructed of steel, were similar to the wings in plan form and cross-section profile, and the ratio of wing exposed area to tail exposed area was 9:1. The tail surfaces in the horizontal plane were all-movable and attached to a steel torque rod. Details of the wing and tail are shown in figure 2.

A hydraulic system supplied by an accumulator was programmed in such a manner as to deflect the control surfaces in a continuous square-wave pattern. The two control positions were 0° and -10° measured with respect to the fuselage center line. At a Mach number of approximately 1.0 the pulse frequency was decreased by means of a switch, which was sensitive to total pressure and controlled the speed of the programming motor.

The physical characteristics of the model are presented in the following table; wing and tail dimensions are the same in the horizontal and vertical planes:

Weight and balance:
Weight, lb 118.6
Center of gravity, percent $\bar{c}$ back of leading edge of $\bar{c}$ . . 9.4
I_Y, slug-ft^2 . . . . 19.8

Wing:
Total wing area in one plane, sq ft 2.89
Exposed wing area in one plane, sq ft 1.73
Mean aerodynamic chord of total wing area, ft 1.49
Mean aerodynamic chord of exposed wing area, ft 1.15
Thickness ratio at wing-body juncture 0.03

Tail surface:
Exposed area in one plane, sq ft 0.19
Mean aerodynamic chord of exposed tail area, ft 0.38
Hinge-line location, percent $\bar{c}_t$ back of leading edge of $\bar{c}_t$ 45.80

Instrumentation

The model was outfitted with an NACA ten-channel telemeter which transmitted a continuous record of normal (2 ranges), longitudinal, transverse, and pitch accelerations, angle of attack, tail deflection, hinge moment, total pressure, and static pressure. Angle of attack was measured by a free-floating vane mounted on a sting, which protruded from the nose of the model. A balance incorporated in the linkage system measured hinge moments about a hinge line located at 45.8 percent of the tail mean aerodynamic chord. Total pressure was obtained by a total-pressure tube extended below the fuselage. A static-pressure orifice was located on the cylindrical section of the body ahead of the wings.

A modified SCR 584 radar tracking unit acquired data on the model trajectory during an early portion of flight. Atmospheric pressure and temperature for the portion of the flight covered by the tracking radar were measured by a radiosonde released shortly after the model flight.

Rate-of-roll information was obtained by a spinsonde receiver in conjunction with the telemeter antenna, which was plane polarized.

TESTS AND ANALYSIS

Tests

The model was launched at a $45°$ elevation angle from a mobile launching platform (fig. 3). Two 6-inch-diameter solid propellant rocket motors of approximately 6,000 pounds of thrust each and 3-second duration boosted the model to supersonic velocity. Test Reynolds numbers based on wing mean aerodynamic chord are shown as a function of Mach number in figure 4. Mach number was determined from the telemetered static and total pressures. Following model-booster separation, the model was disturbed in pitch by a programmed square-wave deflection of the all-movable tail. The transient responses to the step input of the tail were continuously recorded in the form of time histories as the model decelerated through the Mach number range. Sample time histories for a supersonic and a transonic portion of the flight are shown in figure 5.

Analysis

Determination of aerodynamic characteristics.- In the reduction of longitudinal-transient-response data to a step-function input, a method such as that presented in the appendix of reference 2 and based upon the linearized equations of motion is ordinarily utilized to determine longitudinal-stability derivatives and control effectiveness parameters. In such an analysis assumptions of small disturbances, linear aerodynamic coefficients, and constant forward velocity are made. In this investigation some of the aerodynamic characteristics were found to be dependent upon lift, so the results yielded by the methods of reference 2 were average values for the given lift-coefficient ranges. The aerodynamic characteristics determined as average values in this test are P, C_{m_α}, aerodynamic-center location, b, and $C_{m_q} + C_{m_{\dot\alpha}}$. The expression

$$C_{m_\delta} = -C_{m_\alpha} \frac{\Delta\alpha_{trim}}{\Delta\delta}$$ is applicable if the pitching-moment curves for a configuration are linear with angle of attack and control deflection. At Mach numbers above 1.0 the nonlinearity in C_{m_α} was small and C_{m_δ} was determined by using an average of the two C_{m_α} values. As a result of the nonlinear lift-curve slope and the questionable accuracy of C_{L_δ} when the control lift is a small fraction of the model trim lift, C_{L_δ} was

not determined. The hinge-moment derivative C_{h_δ} was determined during
the time of the tail pulse from $C_{h_\delta} = \dfrac{\Delta C_h - C_{h_\alpha} \, \Delta\alpha}{\Delta\delta}$.

<u>Determination of pitching-moment curves</u>.- The pitching-moment equation for two degrees of freedom may be written as

$$C_{m_\alpha}\alpha + C_{m_\delta}\delta = \left(C_m\right)_{\alpha,\delta} = \frac{I_Y\ddot{\theta}}{qSc} - C_{m_q}\frac{c\dot{\theta}}{2V} - C_{m_{\dot{\alpha}}}\frac{c\dot{\alpha}}{2V}$$

Since the damping terms are much smaller than the acceleration term and $\dot{\theta} \approx \dot{\alpha}$ for this test, the pitch equation may be rewritten as

$$\left(C_m\right)_{\alpha,\delta} = \frac{I_Y\ddot{\theta}}{qSc} - \left(C_{m_q} + C_{m_{\dot{\alpha}}}\right)\frac{c\dot{\theta}}{2V}$$

The acceleration and damping terms may be evaluated as time functions by using the previously determined $C_{m_q} + C_{m_{\dot{\alpha}}}$, measured values of $\ddot{\theta}$, and $\dot{\theta}$ determined from an integration of $\ddot{\theta}$. The pitching-moment curve for a given Mach number is obtained by cross-plotting portions of the C_L and $\left(C_m\right)_{\alpha,\delta}$ time histories for a constant tail deflection.

<u>Body bending</u>.- It is known that fuselages of high fineness ratio may experience bending when maneuvering at high normal loads. To determine the amount of body bending for this configuration, calculations were made for the test conditions by considering air and inertia loads and by using estimated values of EI for the fuselage. The results indicate that the wing angle of attack may be greater than the corresponding measured angle of attack by from 1 percent at a Mach number of 0.8 to 6 percent at a Mach number of 1.6, so that an apparent increase in lift-curve slope results.

<u>Coupling effects</u>.- At the higher lift coefficients and at Mach numbers less than 0.88 a coupling of longitudinal and lateral motions is indicated. Shortly after the deflection of the horizontal tail a short-duration rolling velocity of magnitude up to 8 radians/sec was recorded by the spinsonde receiver, followed by an oscillatory transverse acceleration with a magnitude of approximately one-half the normal acceleration. The longitudinal mode maintained damping and periodicity but had a nonlinear trim value which decreased in value during the oscillations.

THEORETICAL CALCULATIONS

With the advent of theories and methods for calculating wing-body and wing-tail interferences, lifts and pitching moments of complete body-wing-tail configurations may be determined by subdividing the problem into the groups:

(1) Lift and pitching moment of body-wing combination.

(2) Lift and pitching moment of body-tail combination.

(3) Wing downwash at the tail location and resultant tail lift and pitching moment.

A general discussion of the methods available for the solution of these component problems, with their limitations and assumptions, is given in reference 5.

In this paper lifts and pitching moments of the body-wing and body-tail combinations were obtained from references 6 and 7, respectively. With the limitation of applicability to angles of attack near zero, the wing downwash field was assumed to be defined by a deflected, unwarped vortex sheet rather than by a pair of fully rolled-up trailing vortices and was calculated from the downwash theory of reference 8. No body or wing viscous effects were included. The force and moment on the tail resulting from the downwash distribution were computed by a modified strip method of reference 9 for wings of subsonic leading edges. These component solutions were then summed to determine the predicted lift and aerodynamic-center location of the complete configuration.

PRECISION OF DATA

Corrections

The angle of attack as measured at the nose was corrected for model pitching velocity and flight-path curvature to obtain the angle at the center of gravity. These methods were described in reference 10.

Since the angular-accelerometer natural frequency was not large compared to the model natural frequency in pitch, it was necessary to consider the instrument frequency-response characteristics in reducing the pitching-acceleration data. The instrument phase lag was determined from an experimental phase-lag—forcing-frequency curve obtained prior to flight and the amplitude-ratio correction was computed from the instrument damping and frequency.

Accuracy

From a consideration of accuracies of the instrumentation and dynamic pressure, the maximum possible errors of M, α, δ, C_L, $C_{D_{min}}$, and C_h are tabulated below as incremental values.

M	Limit of accuracy of -					
	M	α, deg	δ, deg	C_L	$C_{D_{min}}$	C_h
0.8	±0.03	±0.3	±0.1	±0.050	±0.011	--------
1.2	$\pm.02$	$\pm.3$	$\pm.1$	$\pm.030$	$\pm.005$	±0.0016
1.7	$\pm.02$	$\pm.3$	$\pm.1$	$\pm.008$	$\pm.002$	$\pm.0007$

These errors are primarily systematic in nature; for a given time interval the error of any one quantity is a constant increment. Aerodynamic characteristics which are determined from slopes or differences in telemetered quantities are not subjected to these errors.

Calculations have indicated that an additional increment in angle of attack up to $\pm0.5^\circ$ may exist between the angle-of-attack indicator and the center of gravity as a result of body bending due to normal loads.

Although corrections were applied to the pitch-acceleration data as a result of the frequency-response characteristics of the instrument, it is possible that errors in sensitivity and phase angle still exist. Consequently, errors in C_m of ±3 percent of the measured values are believed to be possible.

RESULTS AND DISCUSSION

Static Stability

Lift.- Sample model lift curves, obtained from cross plots of lift coefficient and angle-of-attack time histories, are presented in figure 6. The lift curves are smooth at all Mach numbers but differences in slope may be noted between the lift curves for the different tail deflections. At several Mach numbers a displacement or hysteresis effect may be noted in the data, but it apparently has no effect upon the lift-curve slope.

The slopes of the lift curves were measured and are presented in figure 7. Throughout the Mach number range C_{L_α} is greater at the higher lift coefficients. This difference in C_{L_α} may be attributed to either nonlinear body characteristics or nonlinear downwash, or both. Unpublished tests of this body at a Mach number of 1.62 in the Langley 9-inch supersonic tunnel and calculations including viscous cross-flow effects from the method of reference 11 indicate differences in the body lift-curve slope of the magnitude of the C_{L_α} difference in figure 7. Also, the existence of nonlinear downwash variations with angle of attack for tails located behind delta wings in the extended wing-chord plane has been predicted by theory and shown by wind-tunnel tests (refs. 12 and 13).

Calculations of body bending due to air and inertia loads indicated that the measured C_{L_α} is somewhat greater than that which would have been measured in the case of a rigid body. The computed error in C_{L_α} due to body aeroelasticity varied from 1 percent at a Mach number of 0.8 to 6 percent at a Mach number of 1.6. Theoretical calculations for small angles of attack, in which the concept of a deflected but undistorted vortex sheet was used, are in good agreement with the low-lift data.

To show the effect of tail addition, the C_{L_α} of the tailless delta-wing configuration of reference 1 is compared with the low-lift data of the present model. The C_{L_α} of the model having a tail was greater at all Mach numbers, the difference being from 0.003 to 0.005 at low speeds. With increasing Mach number the difference increases and is 0.010 at a Mach number of 1.60. At this point 50 percent of the difference may be attributed to tail lift and 20 percent may possibly be attributed to a more severe body bending for the tail-configuration model.

Pitching moment.- Period of oscillation of the model is presented in figure 8 for the Mach number range of the investigation. The two curves for different lift-coefficient ranges are indicative of a nonlinear pitching-moment curve. The C_{m_α} curves reduced from these oscillation data are presented in figure 9. The pitching-moment-curve slope is always greater at the higher lift coefficients, with the difference in C_{m_α} varying from 0.0070 at $M = 0.80$ to 0.0008 at $M = 1.70$.

Pitching-moment curves were reduced from the pitch-angular-acceleration data and sample curves are presented in figure 10. The variation of C_m with C_L is smooth except for a Mach number of 0.96 in a small region near zero C_L. This nonlinearity is believed to be attributable to the viscous wake.

The aerodynamic-center location, as determined from the curves of C_{m_α} and C_{L_α}, is presented in figure 11. At supersonic speeds the aerodynamic-center location is the same for both lift-coefficient ranges and shifts rearward only slightly from 39 percent $\bar{c}$ at a Mach number of 1.2 to 42 percent $\bar{c}$ at a Mach number of 1.7. Below a Mach number of 1.2 the curves diverge; the aerodynamic center for the higher lift-coefficient range remains nearly constant at 40 percent $\bar{c}$ and the aerodynamic center for the smaller lift-coefficient range shifts gradually forward to 32 percent $\bar{c}$ at a Mach number of 0.9. The variation of these aerodynamic-center curves suggests that the nonlinear lift curves are attributable predominantly to nonlinear body lift at supersonic speeds and nonlinear downwash at subsonic speeds. The calculated aerodynamic-center location is farther rearward and shifts gradually forward from 57.5 percent $\bar{c}$ at a Mach number of 1.1 to 51 percent $\bar{c}$ at a Mach number of 1.7. The two concepts of a deflected, unwarped vortex sheet or rolled-up trailing vortices yielded calculated aerodynamic-center locations which differed by only 2 percent $\bar{c}$ for this configuration at small angles of attack. To show the effect of tail addition the aerodynamic-center location of the tailless missile of reference 1 is presented. As is seen, the tail had little effect on aerodynamic-center location. Only above a Mach number of 1.2 is the low-angle-of-attack aerodynamic center farther rearward than that of the tailless model.

Dynamic Stability

The variation with Mach number of the exponential damping constant is presented in figure 12. Values of b increase gradually from about 1.0 at a Mach number of 0.90 to about 2.7 at a Mach number of 1.60, and a lift dependency is noted, with b being greater for the higher lift coefficients at all Mach numbers.

The damping-in-pitch derivative $C_{m_q} + C_{m_{\dot{\alpha}}}$ is presented in figure 13 and is seen to be dependent upon lift. Although the possible error of this derivative may be of the order of the difference between the curves, it is believed that the suggested variation with lift is genuine. The damping-in-pitch derivative of the tailless model of reference 1 is presented for comparison. As a result of a more forward center-of-gravity location (3.2 percent $\bar{c}$ more forward) and the presence of a tail, $C_{m_q} + C_{m_{\dot{\alpha}}}$ for the model with the tail is greater through most of the Mach number range.

Control Effectiveness

Longitudinal trim-curves.- The variation of trim angle of attack with Mach number is presented in figure 14 for the two programmed tail

deflections of 0° and -10°. For a tail deflection of -10°, α_{trim} decreases from 6.80° at a Mach number of 0.90 to 5.35° at a Mach number of 1.6. The unexpected variation of α_{trim} on either side of the zero axis for $\delta = 0^\circ$ is possibly due to asymmetries incurred in the construction of the model and out of trim in the angle-of-attack indicator.

The variation of trim lift coefficient with Mach number for $\delta = 0^\circ$ and -10° is presented in figure 15. The trend of the $C_{L_{trim}}$ curves is similar to that of the α_{trim} curves with decreasing values as the Mach number increases. However, the values of $C_{L_{trim}}$ at $\delta = 0^\circ$ remain slightly negative over the range of Mach number of this test.

Trim angle of attack and lift coefficient per unit control deflection.-
From figure 14 the trim angle of attack per unit control deflection is determined and presented in figure 16 as a function of Mach number. The curve of $\Delta\alpha_{trim}/\Delta\delta$ diminishes sharply between $M = 0.9$ and $M = 1.05$ from a value of -0.71 to -0.58 followed by an almost linear decrease to -0.48 at $M = 1.6$.

The change in trim lift coefficient due to a unit control deflection, which was determined in the same manner as $\Delta\alpha_{trim}/\Delta\delta$, is presented in figure 17. A comparison is made between the model of the test, a tip-control model (ref. 1) and a canard model (ref. 2). The ratio of control area to wing area is the same for all three models. For the all-movable tail model the variation of $\Delta C_{L_{trim}}/\Delta\delta$ with M is nearly linear, decreasing from -0.036 at $M = 0.8$ to -0.020 at $M = 1.6$. The values of $\Delta C_{L_{trim}}/\Delta\delta$ of this model are higher than those of the tip-control model by a factor of 2.2 at $M = 0.8$, 3.8 at $M = 1.2$, and 2.8 at $M = 1.6$, even though the static stability is greater. Although $\Delta C_{L_{trim}}/\Delta\delta$ is of nearly the same magnitude for the test model and the canard model, the test model is favored by a static stability approximately 30 percent lower than that of the canard model.

Tail pitching effectiveness.- The pitching effectiveness is plotted as a function of Mach number in figure 18. A comparison with theoretical results obtained by application of the method of reference 14 indicates good agreement. The small difference between test and theory may result from dynamic-pressure changes at the tail due to the viscous wake. At test Mach numbers above 1.1 the trend of C_{m_δ} for the model of this test and the tip-control model are quite similar. However, the control of the test model was decidedly more effective in producing pitch with a value of C_{m_δ} three times as great at $M = 1.1$ and four times as great at $M = 1.6$. The pitching effectiveness of the canard model is of

opposite sign to that of the all-movable-tail model and of greater mag-
nitude. At $M = 1.0$ C_{m_δ} for the canard model is 43 percent greater
than that for the test model and 40 percent larger at $M = 1.45$, although
the moment arm from the center of gravity to the control surface is some-
what greater for the all-movable-tail model than the canard model. The
higher value of C_{m_δ} for the latter is attributed to a reduction in the
wing stabilizing moment caused by downwash due to control deflection.

Hinge Moments

Tail hinge moments were measured about an axis at 46 percent $\bar{c}_t$.
The maximum hinge moment recorded was 2.8 foot-pounds at a Mach number
of 1.56, angle of attack of 4.9°, and tail deflection of -10°.

Hinge-moment-coefficient curves are presented in figure 19 at con-
stant tail deflections of 0° and -10°. Although the hinge-moment coef-
ficient is nonlinear at all Mach numbers, some consistent trends are noted.
At low angles of attack and a tail deflection of 0°, C_h is nearly linear
at all Mach numbers and always has a positive slope. At high angles of
attack and a control deflection of -10° two changes in slope are noted.
For the Mach number range from 1.56 to 1.03 the slope of C_h with angle
of attack is positive for $3° < \alpha < 5°$ and negative for $5° < \alpha < 8°$. At Mach
numbers of 1.03 and 0.90 the slope becomes positive again as still greater
angles of attack are attained. Changes in slope of C_h with α indicate
tail center-of-pressure shifts in which the negative slope experienced in
the range $5° < \alpha < 8°$ indicates a rearward movement of the center of pressure.
These center-of-pressure shifts are believed to be attributable to the non-
uniform flow field produced by the wing and to an angle-of-attack effect
upon the basic pressure distribution.

Hinge-moment coefficient derivatives C_{h_δ} and C_{h_α} for small angles
of attack are presented in figure 20. At subsonic speeds both C_{h_δ}
and C_{h_α} are positive and of same magnitude. As Mach number increases,
C_{h_δ} decreases and becomes zero at a Mach number of 1.21, at which time
the center of pressure due to δ is on the hinge line. At higher Mach
numbers the center of pressure due to δ is slightly rearward of the
hinge line. After decreasing some at transonic speeds, C_{h_α} remains
nearly constant at supersonic speeds. Some effects of the wake may be
obtained by comparing these derivatives with the canard-control hinge-
moment data of reference 2. No comparison of actual control centers of
pressure is afforded since control lift characteristics were not measured,

but it is noteworthy that the Mach number trends of C_{h_α} and C_{h_δ} are similar for both controls. At supersonic speeds the derivatives are of the same magnitude, but at subsonic speeds the hinge-moment derivatives of the all-movable tail were smaller than for the canard control.

Drag

Although the primary purpose of this investigation was to determine longitudinal stability and control characteristics of the missile, drag was also measured and is presented in several forms herein.

Drag polars from $M = 0.79$ to $M = 1.70$ are presented in figure 21. The variation of C_D with C_L was parabolic as expected for the condition of $\delta = -10°$. The shape of the drag polars for $\delta = 0°$ results from changes in the chord force, which are evident in the longitudinal-acceleration time history of figures 5(a) and 5(b).

The maximum lift-drag ratio, which was determined directly from the drag polars, is presented in figure 22 from $M = 0.82$ to $M = 1.09$. The model did not attain the condition of $(L/D)_{max}$ at supersonic speeds. The $(L/D)_{max}$ decreases sharply from 5.85 at $M = 0.82$ to 3.60 at $M = 0.95$ and then remains almost constant to a value of 3.55 at $M = 1.09$.

The drag coefficient at zero lift as presented in figure 23 indicates a sharp drag rise from $C_D = 0.020$ at $M = 0.85$ to $C_D = 0.061$ at $M = 1.07$. There is a gradual decrease in drag coefficient through the supersonic region to a value of 0.044 at $M = 1.70$. Although the drag polars for $\delta = 0°$ were irregular in appearance, the drag measurements appear to be of the correct level as shown by the good agreement of $C_{D_{min}}$ with that of the canard model.

CONCLUSIONS

The results of a flight investigation at Mach numbers 0.67 to 1.81 of a cruciform, delta-wing missile having an all-movable horizontal tail and comparisons with a delta-wing missile having half-delta tip controls indicate the following conclusions:

1. Nonlinear lift and pitching-moment curves were indicated from the data measured at two ranges of angle of attack. At supersonic speeds the aerodynamic-center location remains nearly constant at 40 percent of the wing mean aerodynamic chord $\bar{c}$ for both angle-of-attack ranges. As the

Mach number decreases, the aerodynamic-center location for the higher
lift-coefficient range remains at 40 percent $\bar{c}$ while for the lower range
it shifts forward to 32 percent $\bar{c}$ at a Mach number of 0.9.

2. The lift-curve slope of the all-movable-tail configuration is
greater by 0.003 to 0.010 than the tailless configuration. The tail had
little effect on the aerodynamic-center location except at higher super-
sonic speeds where the aerodynamic center of the tail configuration was
farther rearward.

3. Calculations, in which the downstream flow field was assumed to
be defined by a deflected, unwarped vortex sheet, were in agreement with
the low angle-of-attack lift-curve slope but predicted a more rearward
aerodynamic-center location of 9 to 18 percent $\bar{c}$.

4. The damping-in-pitch derivative $C_{m_q} + C_{m_{\dot{\alpha}}}$ was dependent upon
lift at all but the peak Mach number and was greater for the large lift-
coefficient range. From near zero at a Mach number of 0.9, $C_{m_q} + C_{m_{\dot{\alpha}}}$
increased rapidly to a peak value at a Mach number of 1.2 and then
decreased gradually with further increasing Mach number.

5. The all-movable tail was effective in producing pitching moment,
with the pitching-effectiveness derivative C_{m_δ} being three to four
times as great as for the tip control. The model trim lift per unit tail
deflection $\Delta C_{L_{trim}}/\Delta\delta$ was larger by 2.2 to 3.8 times that resulting
from the tip-control deflection. The values of $\Delta C_{L_{trim}}/\Delta\delta$ decreased
with increasing Mach number and experienced a reduction of 45 percent
with increase in Mach number from 0.8 to 1.6.

6. At low angles of attack the hinge-moment-coefficient variation
with angle of attack was nearly linear and had a small positive slope.
At angles of attack greater than $5°$ center-of-pressure changes were
denoted by abrupt changes in slope at all Mach numbers.

Langley Aeronautical Laboratory,
    National Advisory Committee for Aeronautics,
        Langley Field, Va., July 31, 1953.

REFERENCES

1. Moul, Martin T., and Baber, Hal T., Jr.: The Longitudinal Stability and Control Characteristics of a 60° Delta-Wing Missile Having Half-Delta Tip Controls As Obtained From a Free-Flight Investigation at Transonic and Supersonic Speeds. NACA RM L52H14, 1952.

2. Niewald, Roy J., and Moul, Martin T.: The Longitudinal Stability, Control Effectiveness, and Control Hinge-Moment Characteristics Obtained From a Flight Investigation of a Canard Missile Configuration at Transonic and Supersonic Speeds. NACA RM L50I27, 1950.

3. Brown, Clarence A., Jr., and Lundstrom, Reginald R.: Flight Investigation From Mach Number 0.8 to Mach Number 2.0 To Determine Some Effects of Wing-to-Tail Distance on the Longitudinal Stability and Control Characteristics of a 60° Delta-Wing - Canard Missile. NACA RM L52C26, 1952.

4. Moul, Martin T., and Wineman, Andrew R.: Longitudinal Stability and Control Characteristics From a Flight Investigation of a Cruciform Canard Missile Configuration Having an Exposed Wing-Canard Area Ratio of 16:1. NACA RM L52D24a, 1952.

5. Edwards, S. Sherman: Experimental and Theoretical Study of Factors Influencing the Longitudinal Stability of an Air-to-Air Missile at a Mach Number of 1.4. NACA RM A51J19, 1952.

6. Nielsen, Jack N., and Kaattari, George E.: Method for Estimating Lift Interference of Wing-Body Combinations at Supersonic Speeds. NACA RM A51J04, 1951.

7. Kaattari, George E., Nielsen, Jack N., and Pitts, William C.: Method for Estimating Pitching-Moment Interference of Wing-Body Combinations at Supersonic Speed. NACA RM A52B06, 1952.

8. Lagerstrom, P. A., Graham, Martha E., and Grosslight, G.: Downwash and Sidewash Induced by Three-Dimensional Lifting Wings in Supersonic Flow. Rep. No. SM-13007, Douglas Aircraft Co., April 14, 1947.

9. Graham, Martha E.: Some Linearized Computations of Supersonic Wing-Tail Interference. Rep. No. SM-13430, Douglas Aircraft Co., Inc., Dec. 23, 1948.

10. Mitchell, Jesse L., and Peck, Robert F.: An NACA Vane-Type Angle-of-Attack Indicator for Use at Subsonic and Supersonic Speeds. NACA RM L9F28a, 1949.

CONFIDENTIAL

11. Allen, H. Julian: Estimation of the Forces and Moments Acting on Inclined Bodies of Revolution of High Fineness Ratio. NACA RM A9I26, 1949.

12. Perkins, Edward W., and Canning, Thomas N.: Investigation of Downwash and Wake Characteristics at a Mach Number of 1.53. II - Triangular Wing. NACA RM A9D20, 1949.

13. Graham, David, and Koenig, David G.: Tests in the Ames 40- by 80-Foot Wind Tunnel of an Airplane Configuration With an Aspect Ratio 2 Triangular Wing and an All-Movable Horizontal Tail - Longitudinal Characteristics. NACA RM A51B21, 1951.

14. Nielsen, Jack N., Kaattari, George E., and Drake, William C.: Comparison Between Prediction and Experiment for All-Movable Wing and Body Combinations at Supersonic Speeds - Lift, Pitching Moment, and Hinge Moment. NACA RM A52D29, 1952.
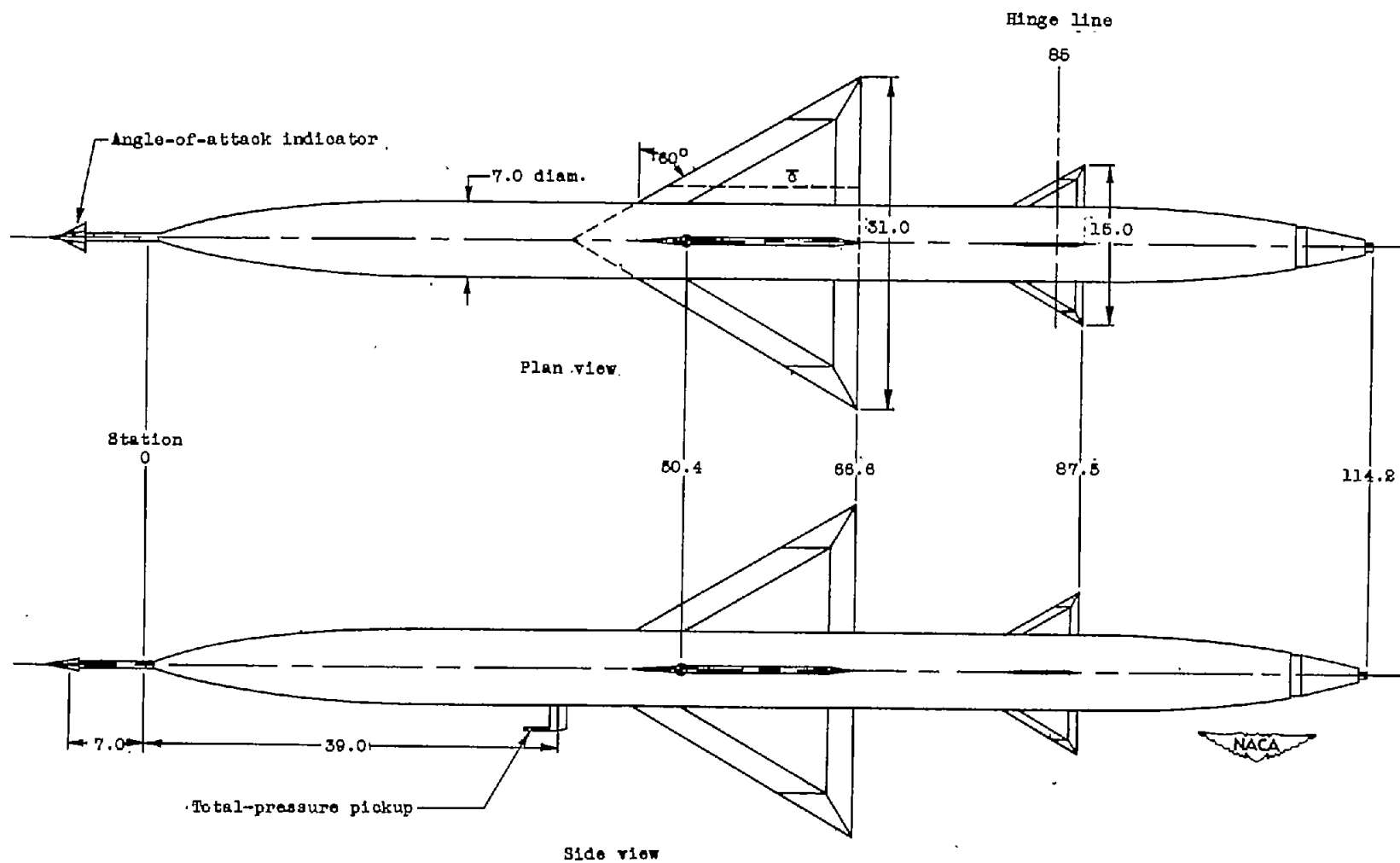
Figure 1.- Model arrangement. All dimensions are in inches.

CONFIDENTIAL

Section A-A
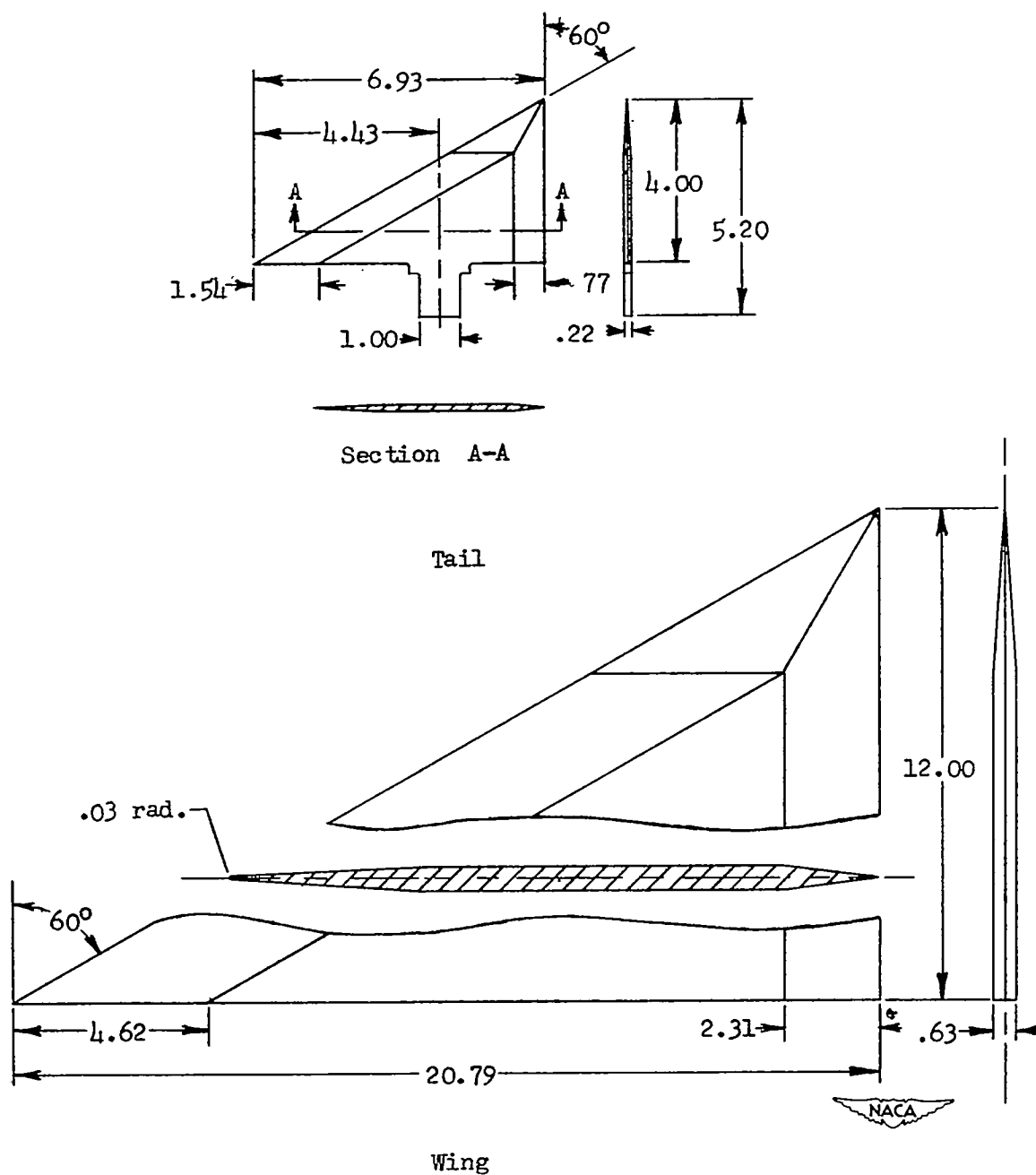
Tail

Wing

Figure 2.- Detail of wing and tail. All dimensions are in inches.
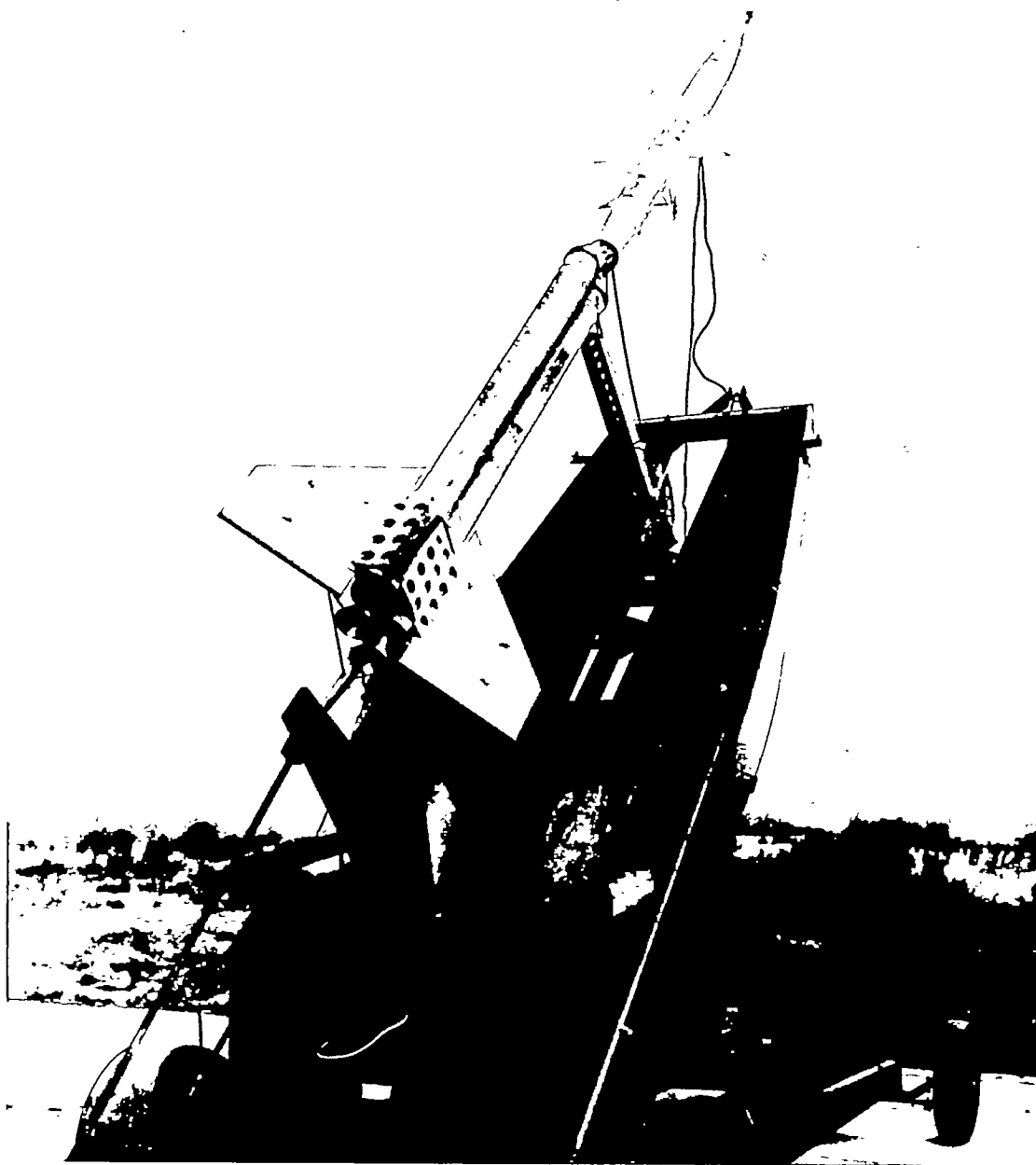
CONFIDENTIAL

Figure 3.- Model-booster combination at launch.

L-73768.1
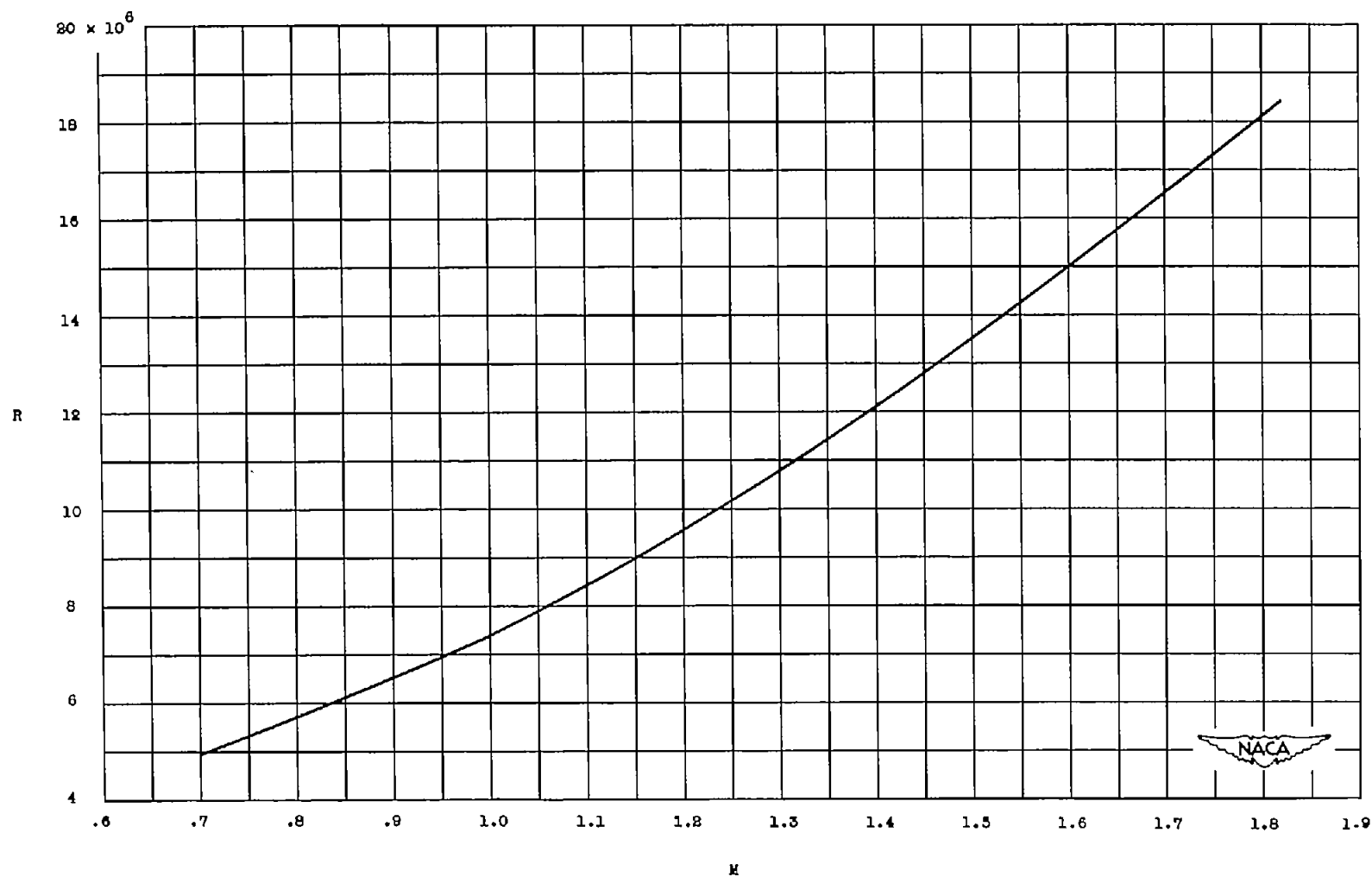
Figure 4.- Variation with Mach number of Reynolds number based on wing
mean aerodynamic chord of 1.49 feet.

CONFIDENTIAL
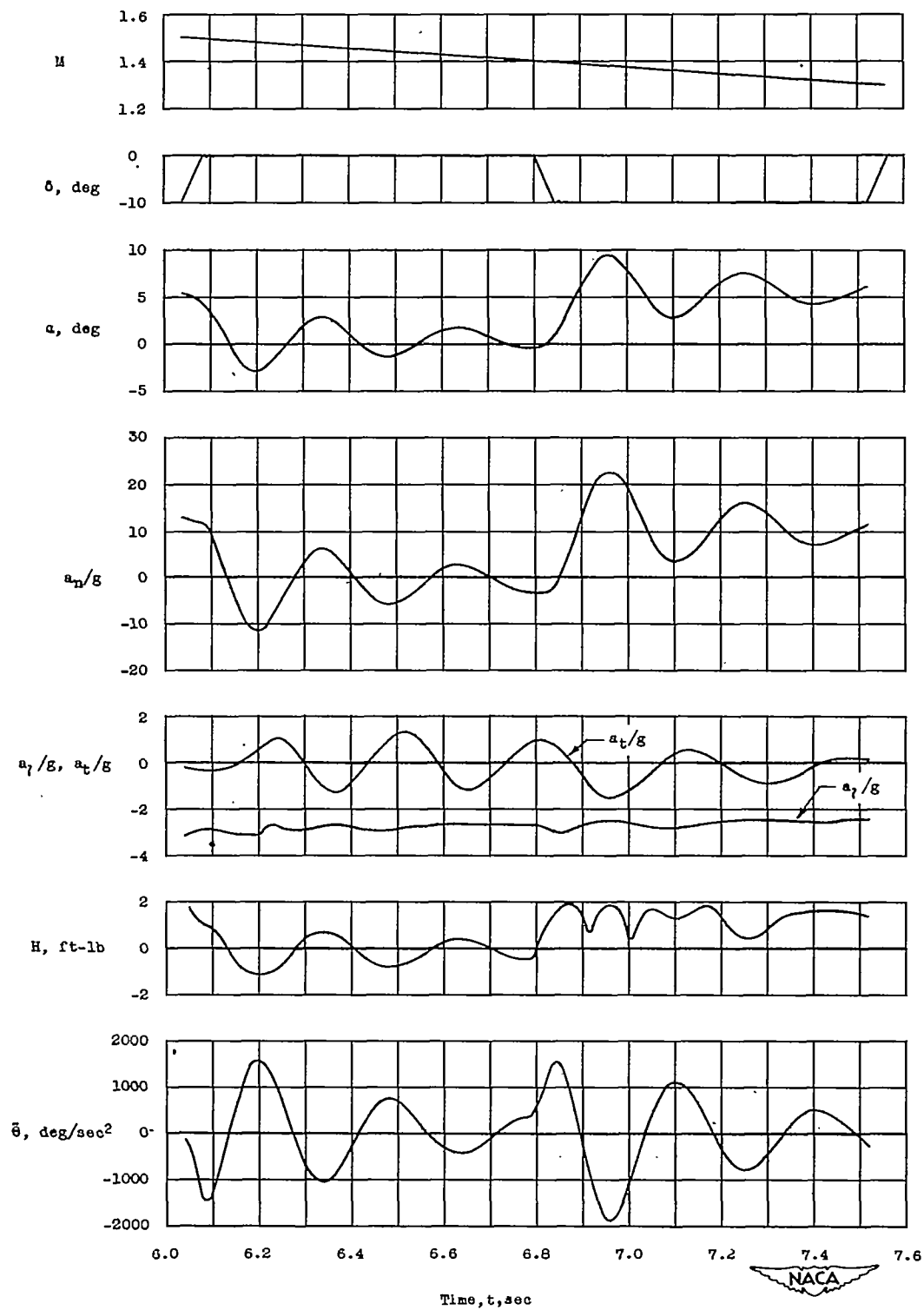
(a) Supersonic.

Figure 5.- Sample time histories of model flight.
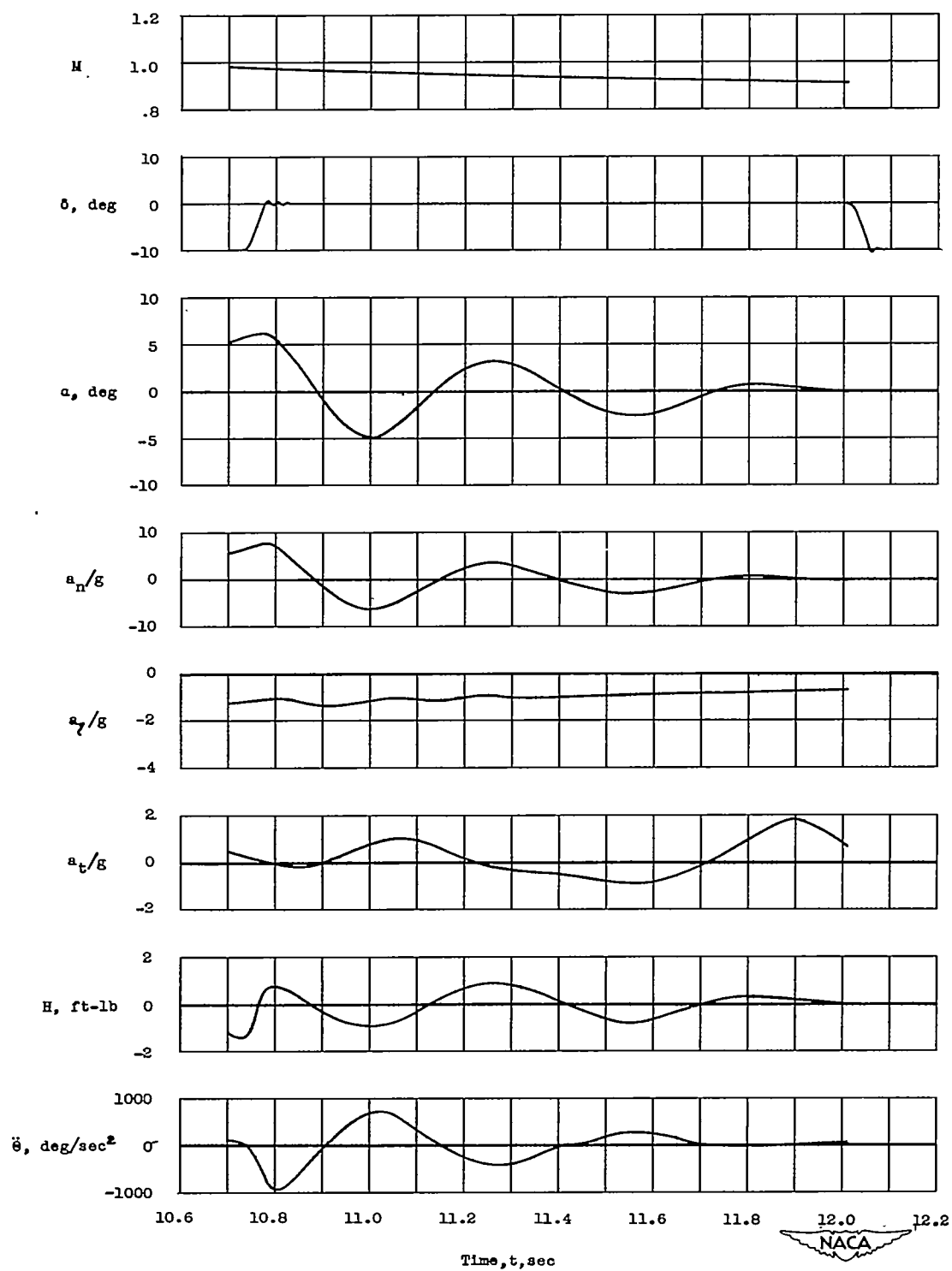
(b) Transonic.

Figure 5.- Concluded.
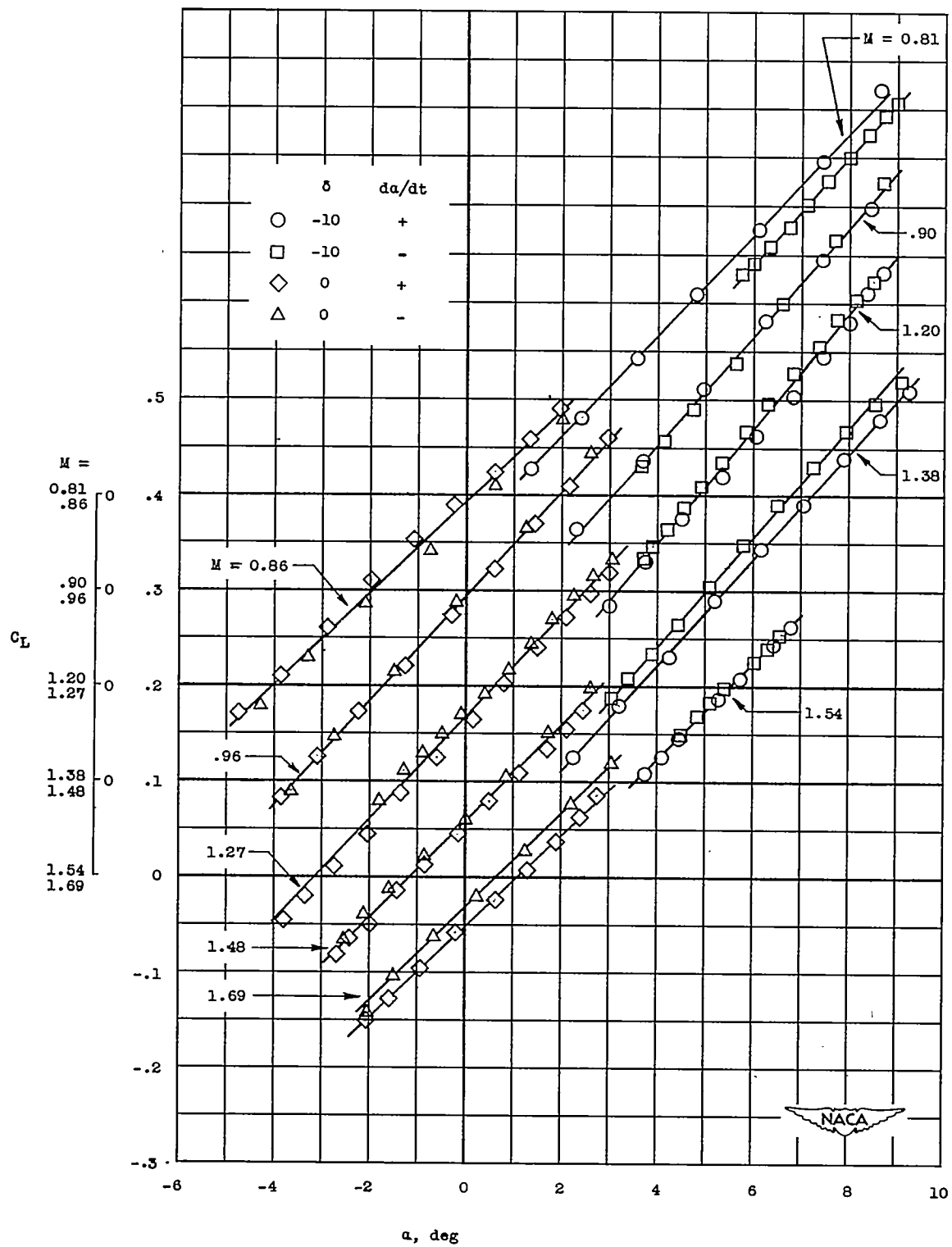
Figure 6.- Typical model lift curves.
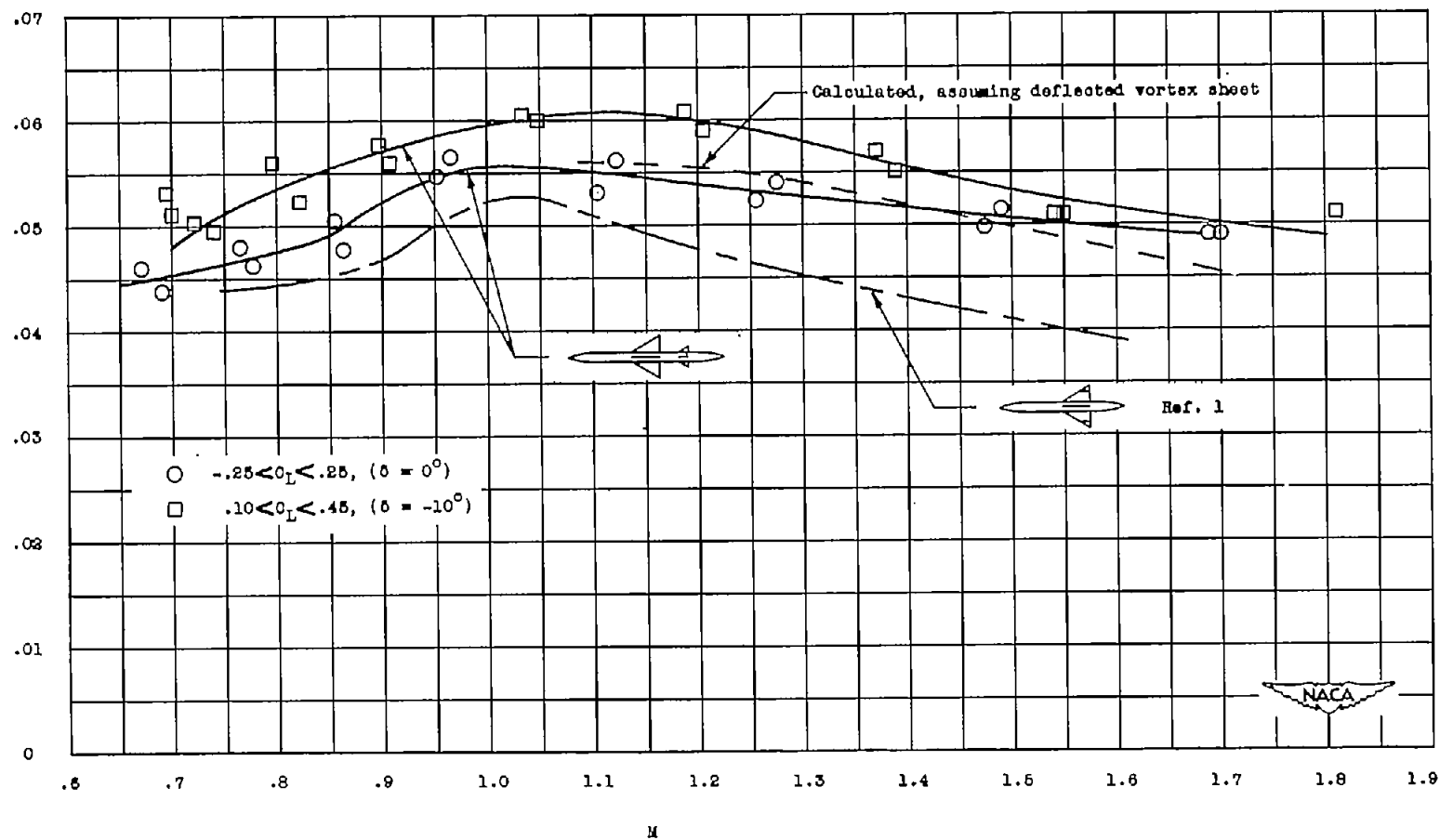
Figure 7.- Variation of model lift-curve slope with Mach number for two
ranges of lift coefficient.
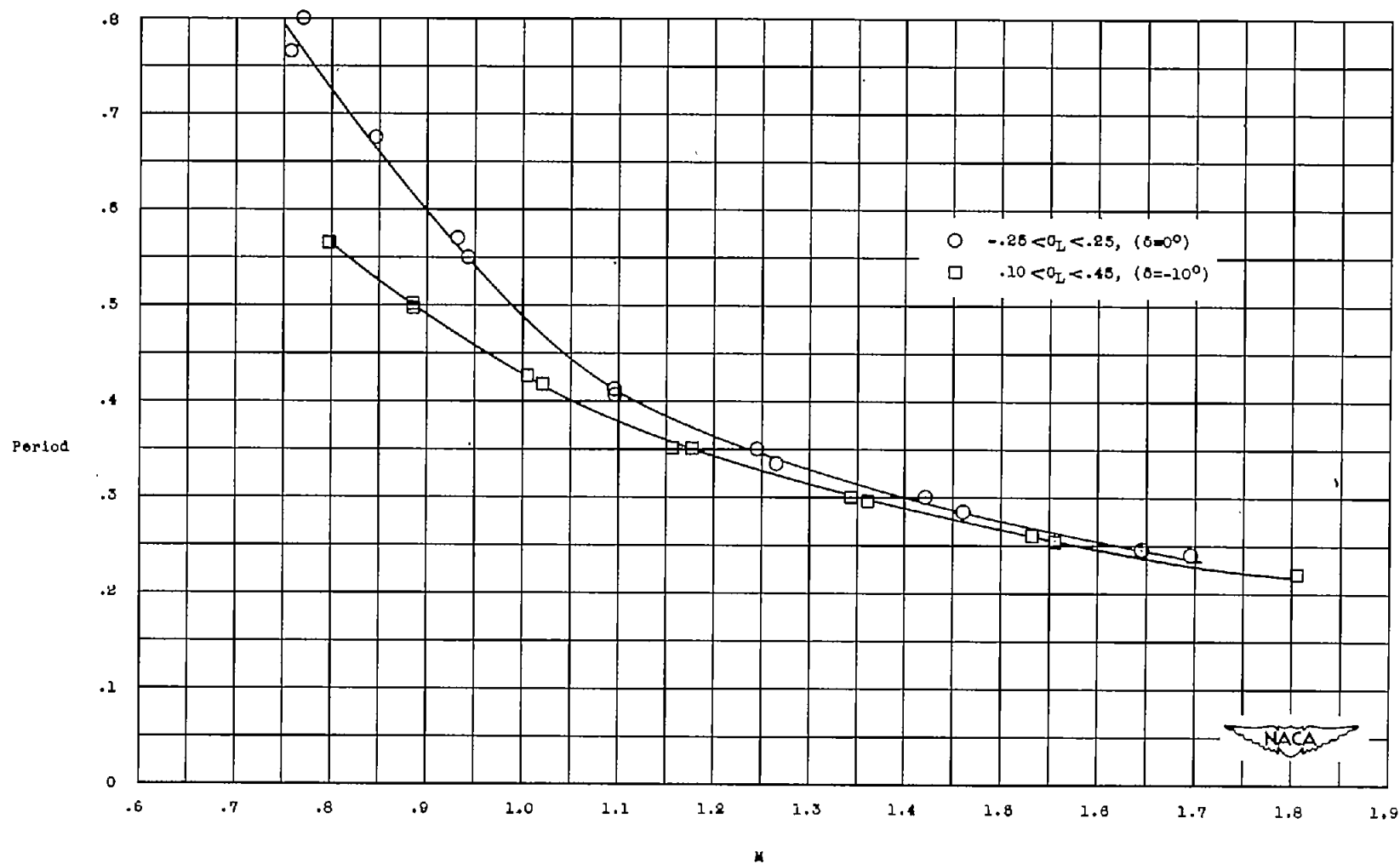
Figure 8.- Variation of period with Mach number.
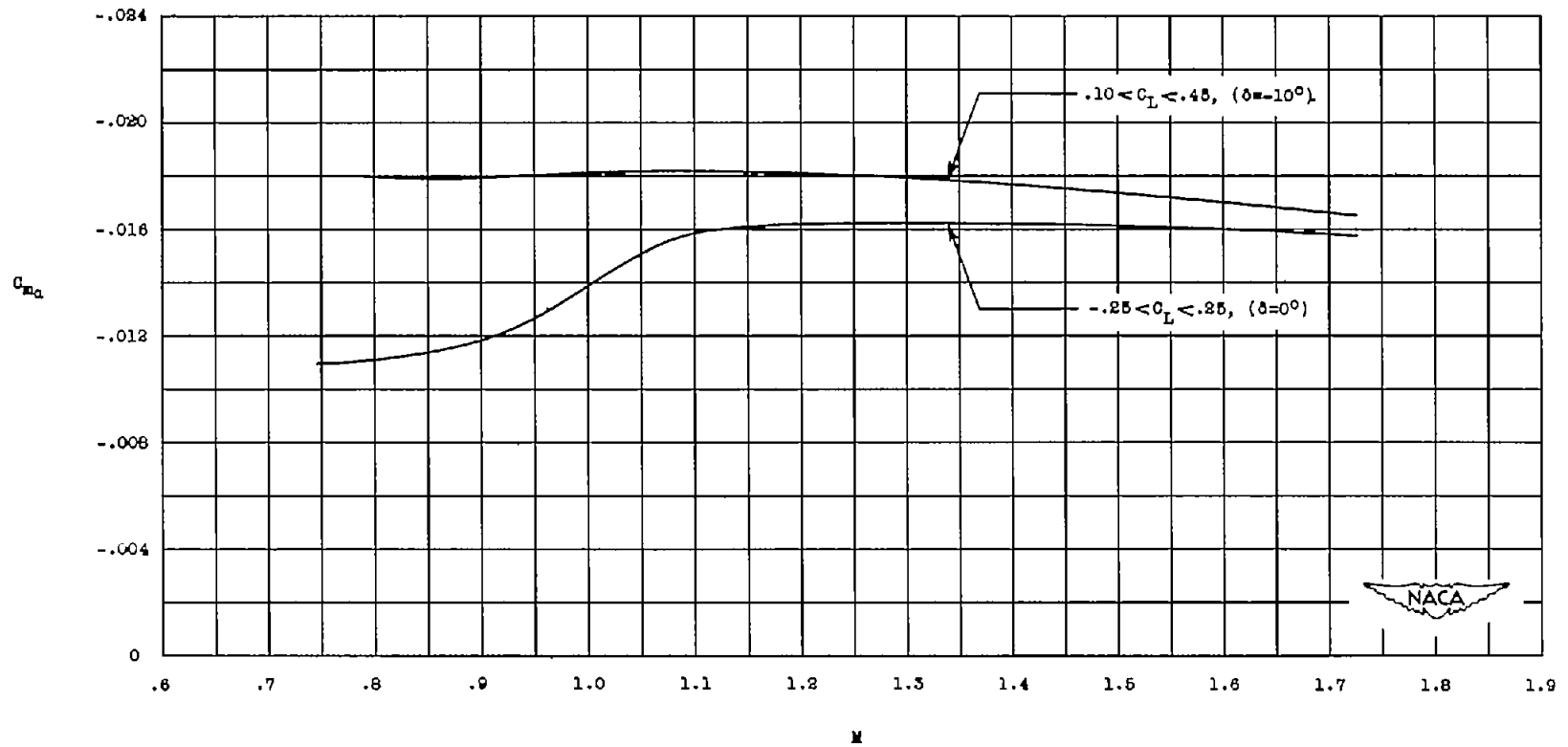
Figure 9.- Variation of C_{m_α} with Mach number for two ranges of lift coefficient.

CONFIDENTIAL
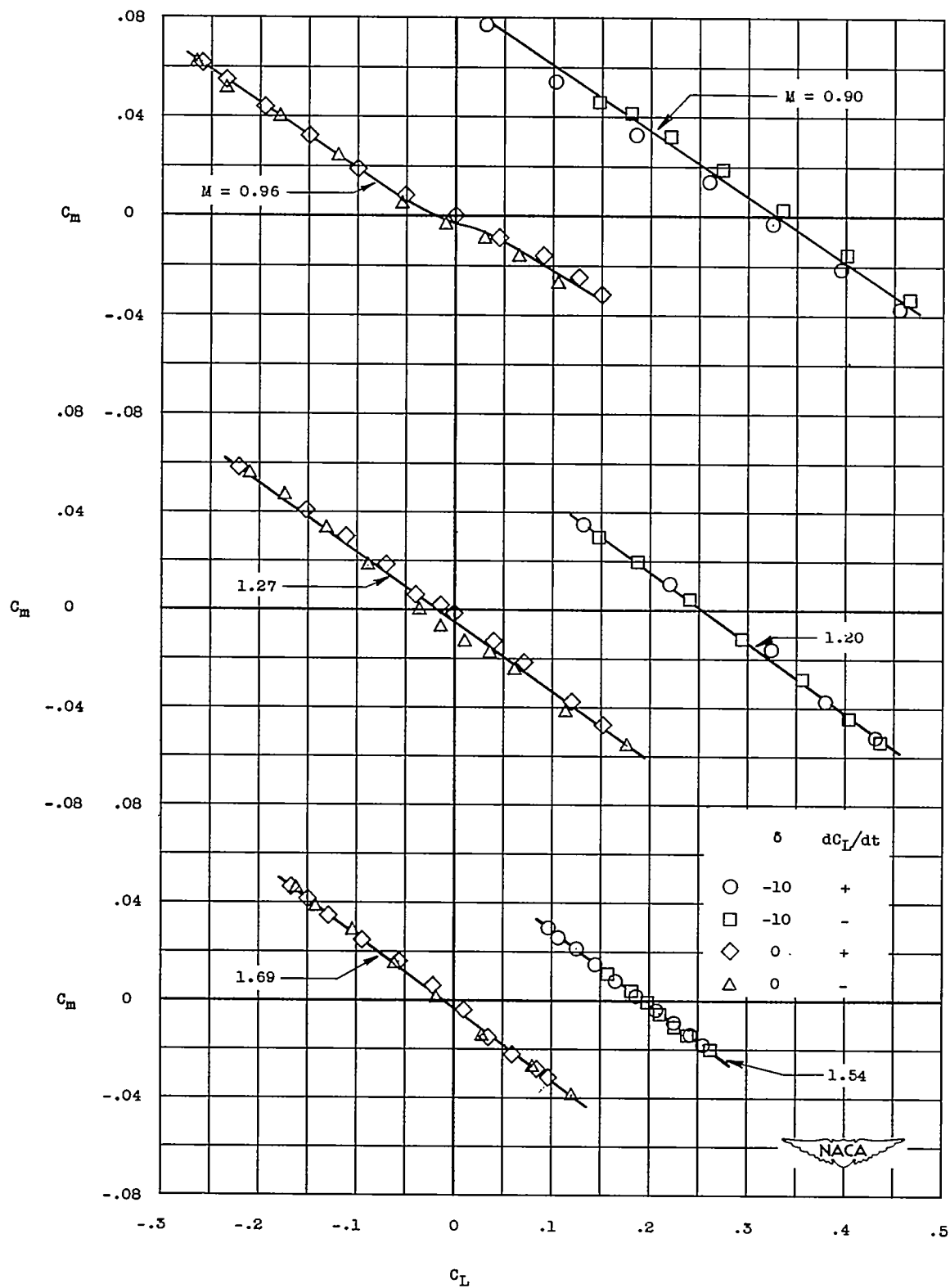
Figure 10.- Sample pitching-moment curves.
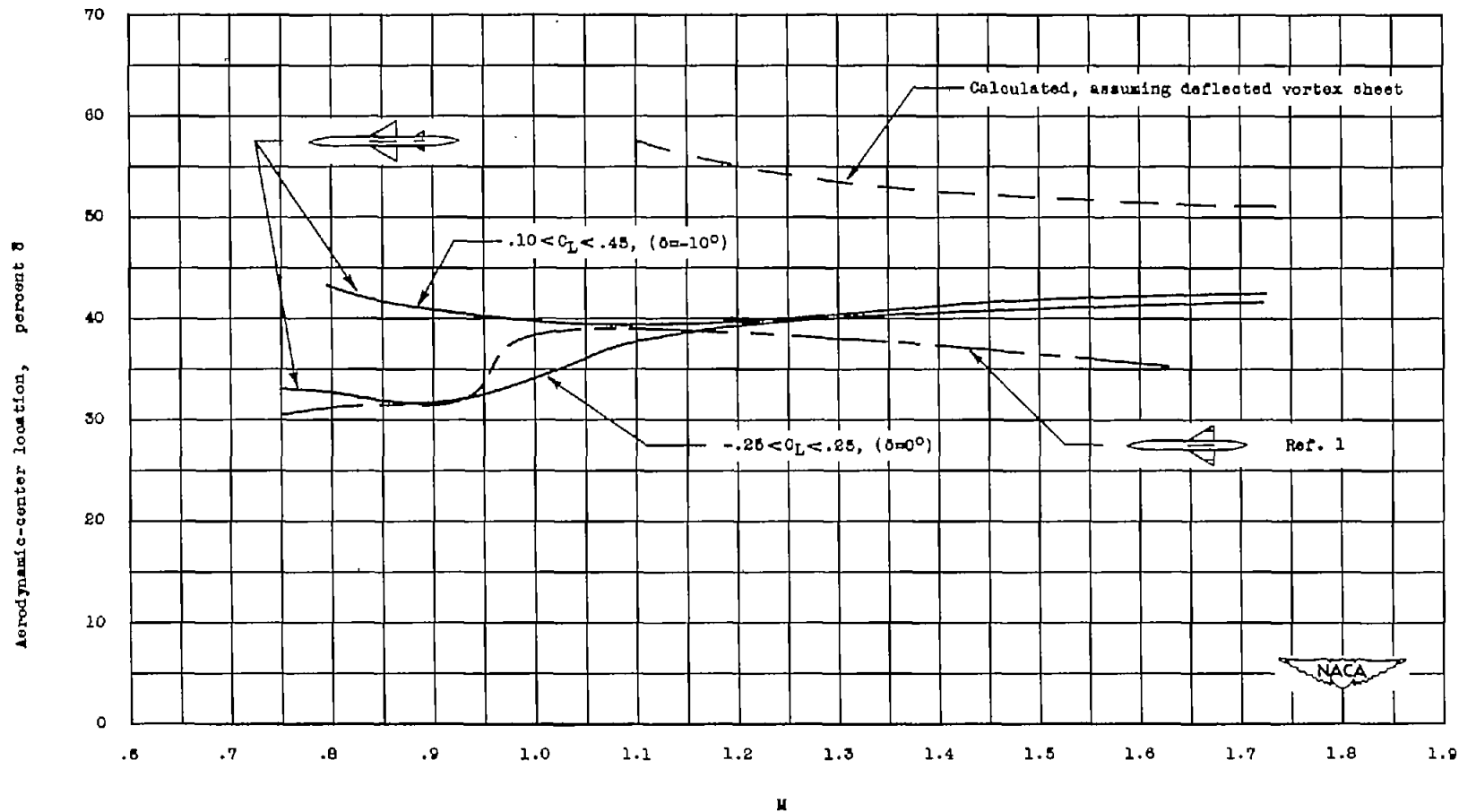
Figure 11.- Variation of aerodynamic-center location with Mach number for two ranges of lift coefficient.
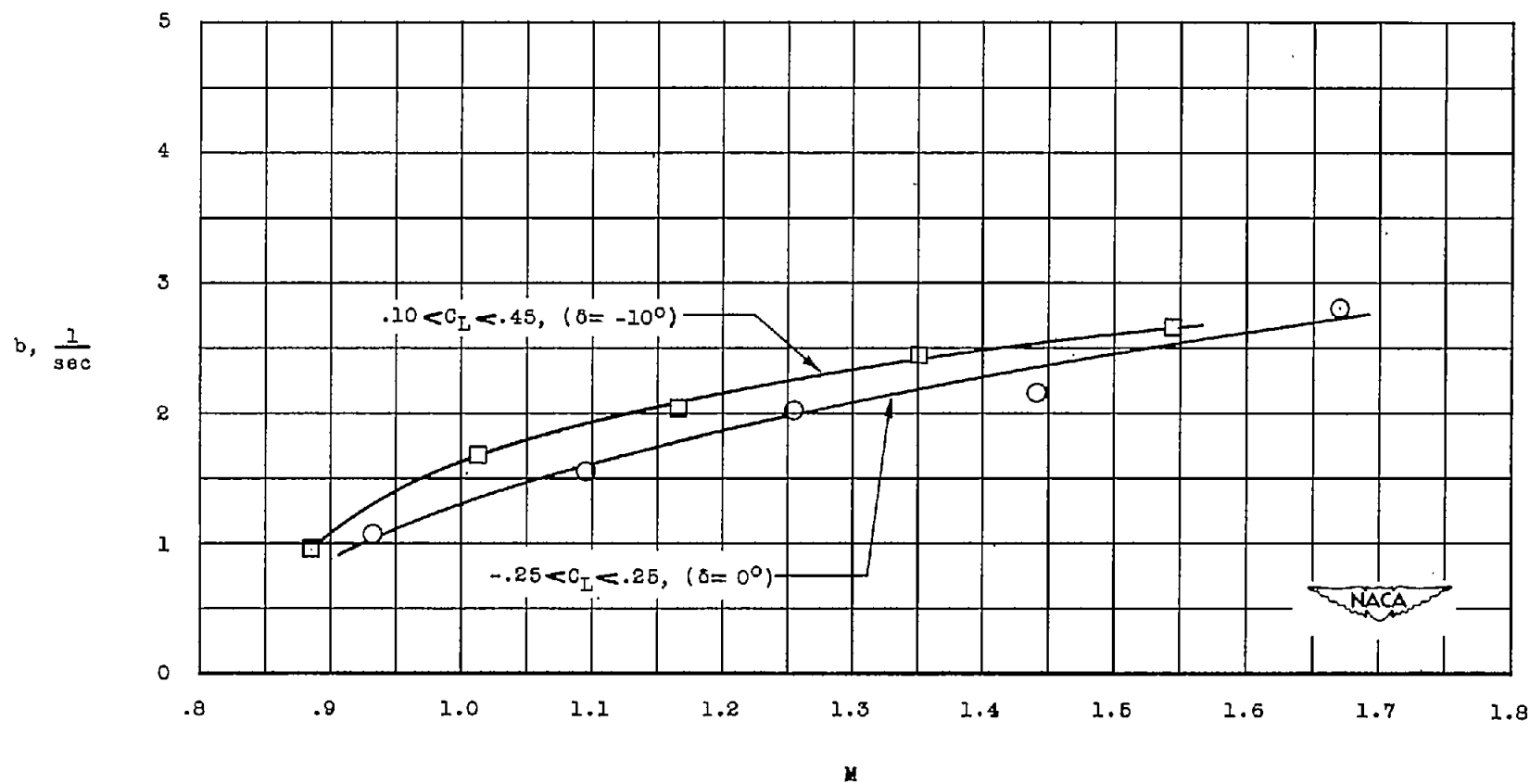
Figure 12.- Variation of exponential damping constant b with Mach number.
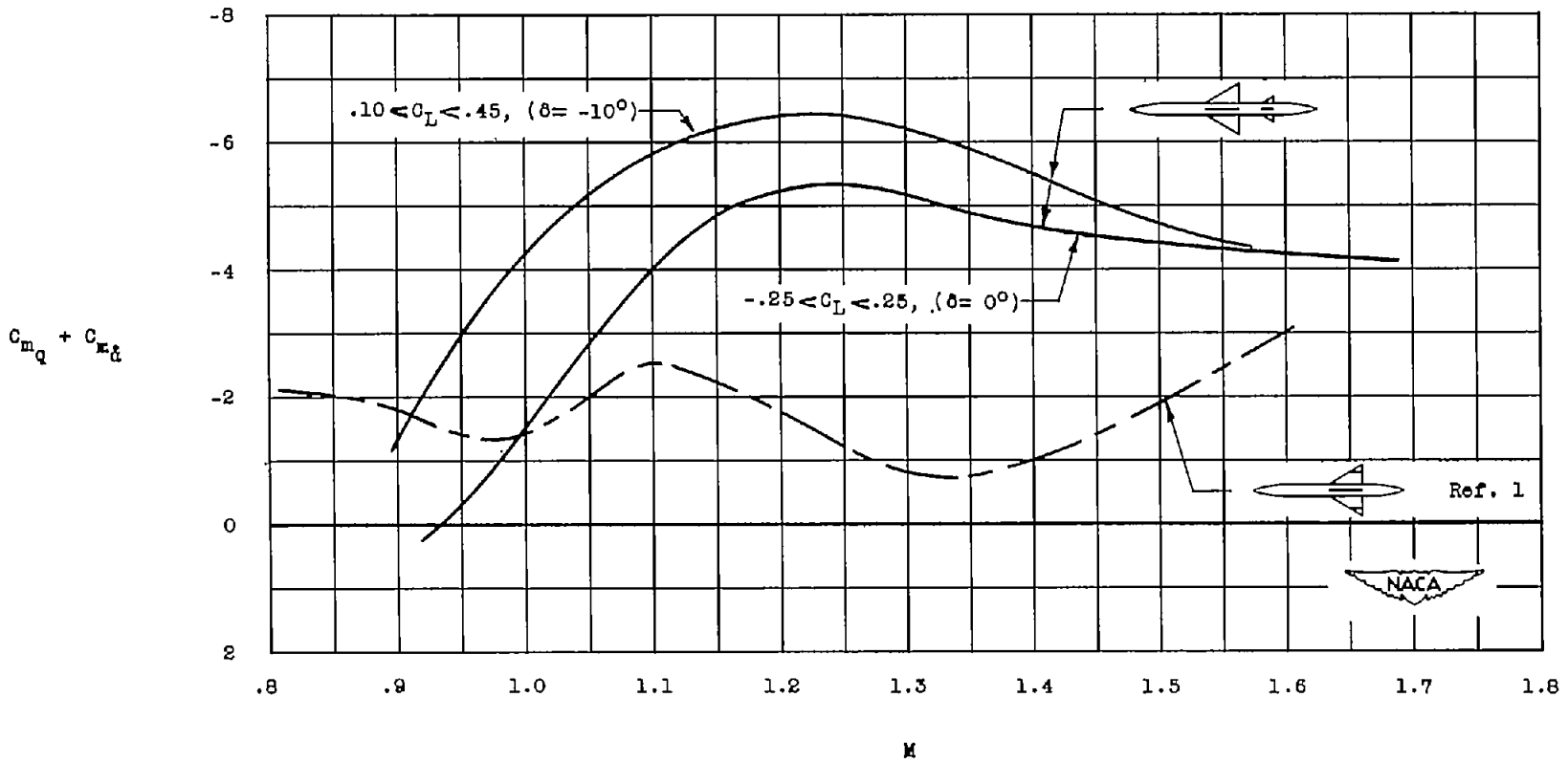
Figure 13.- Variation of aerodynamic damping-in-pitch derivative with Mach number.

α_{trim}, deg
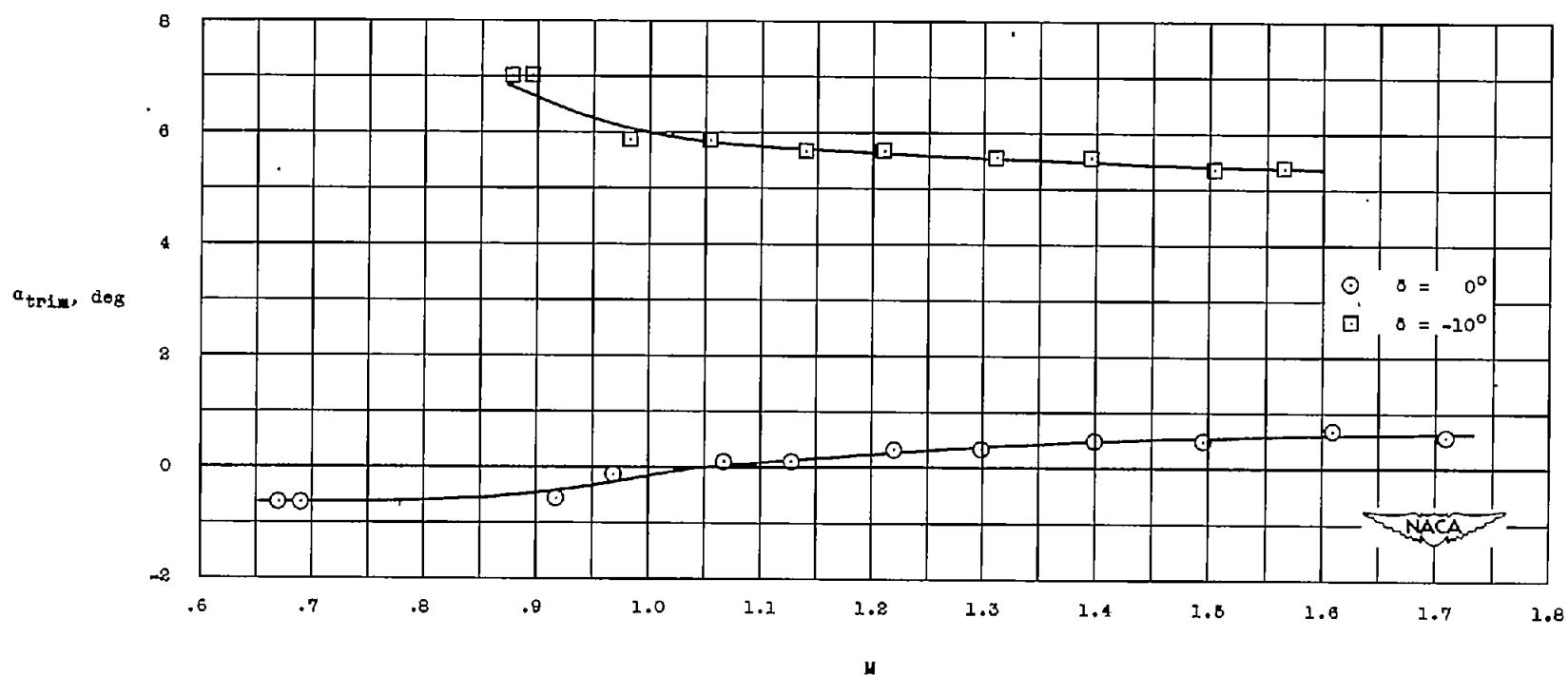
Figure 14.- Variation of trim angle of attack with Mach number.
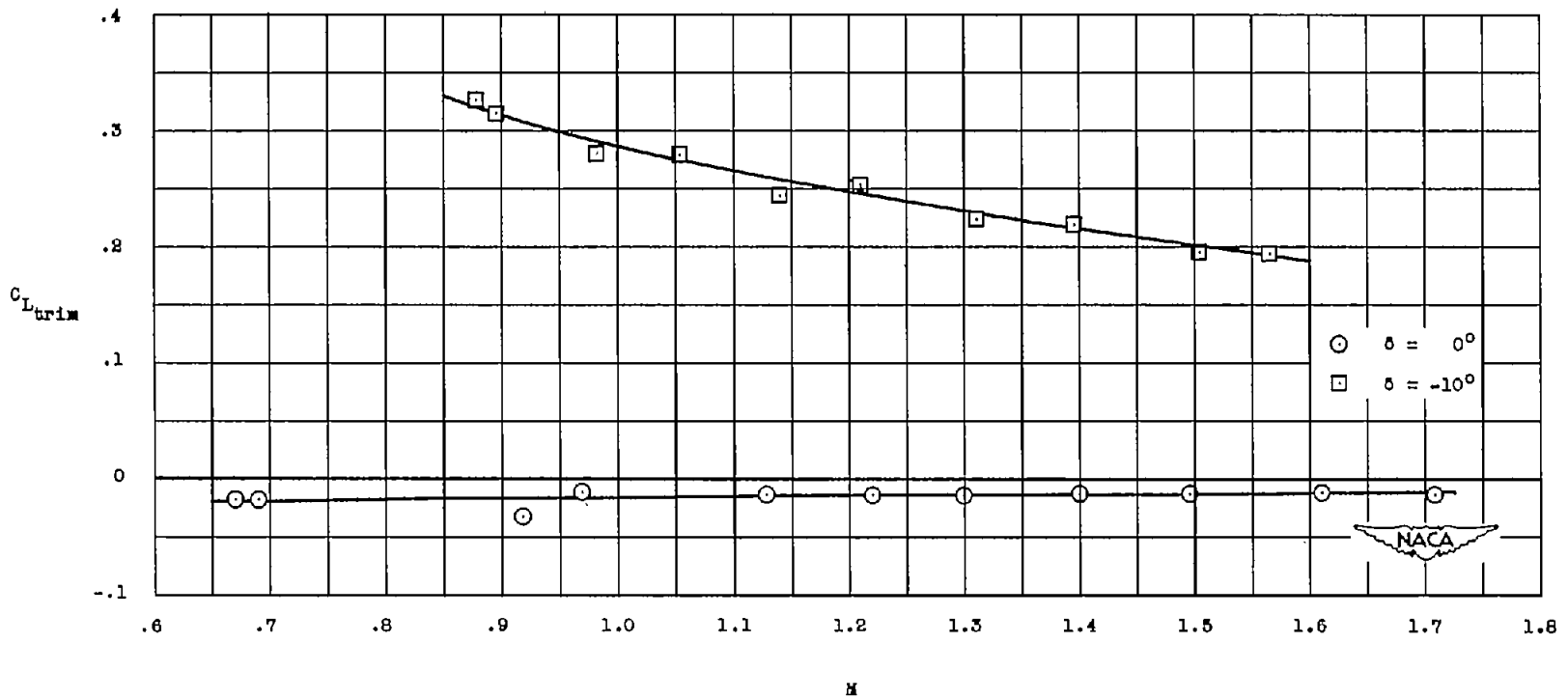
Figure 15.- Variation of trim lift coefficient with Mach number.
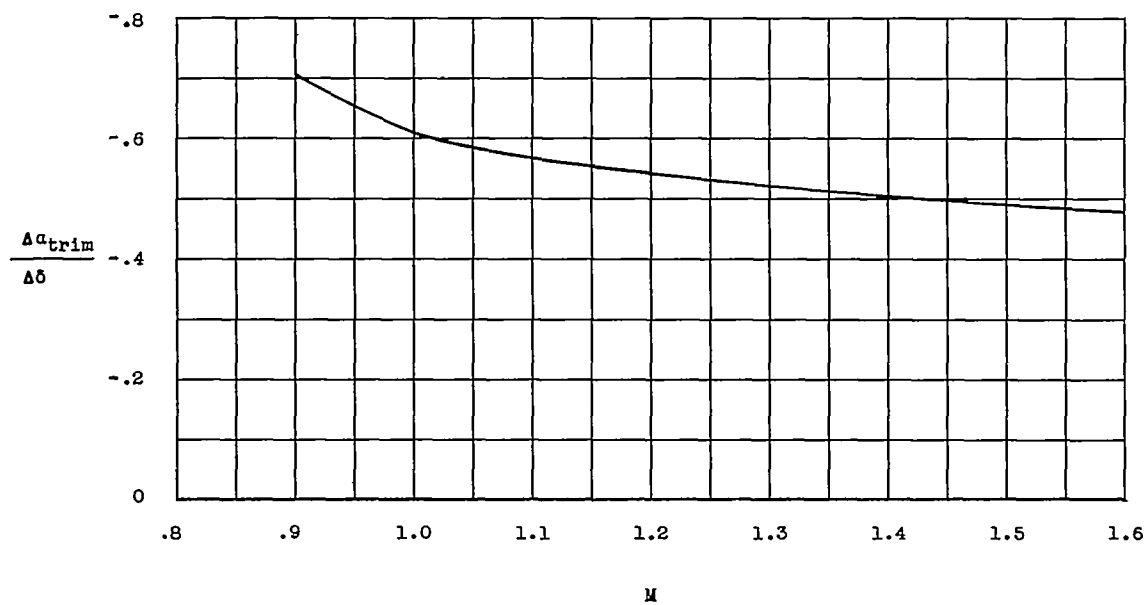
Figure 16.- Trim angle of attack produced by a unit control deflection.
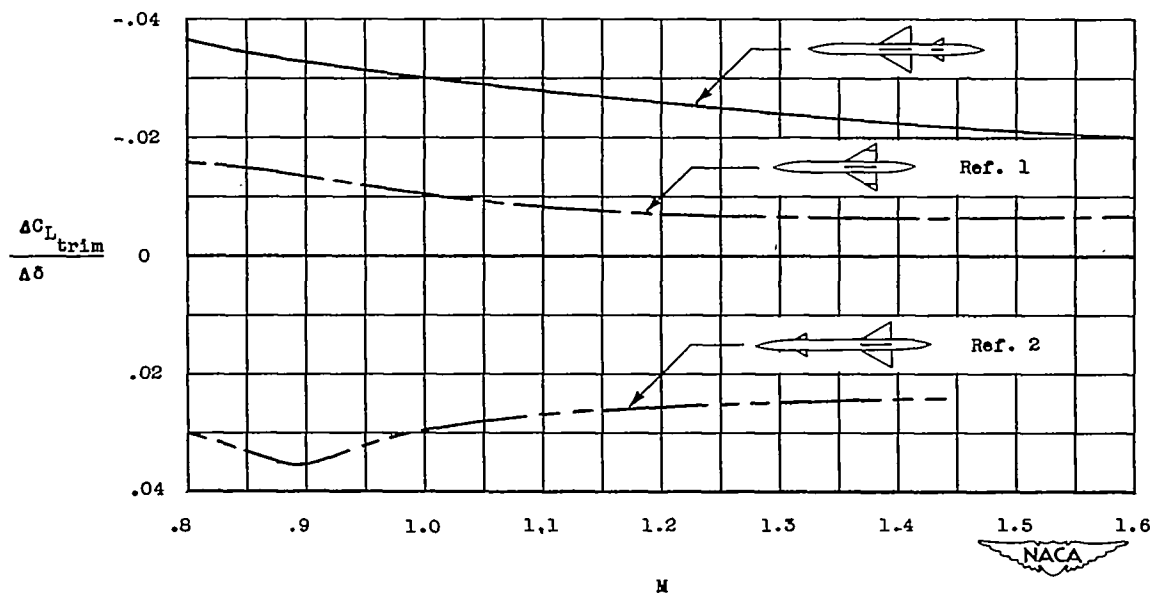
Figure 17.- Variation with Mach number of trim lift coefficient due to control deflection.
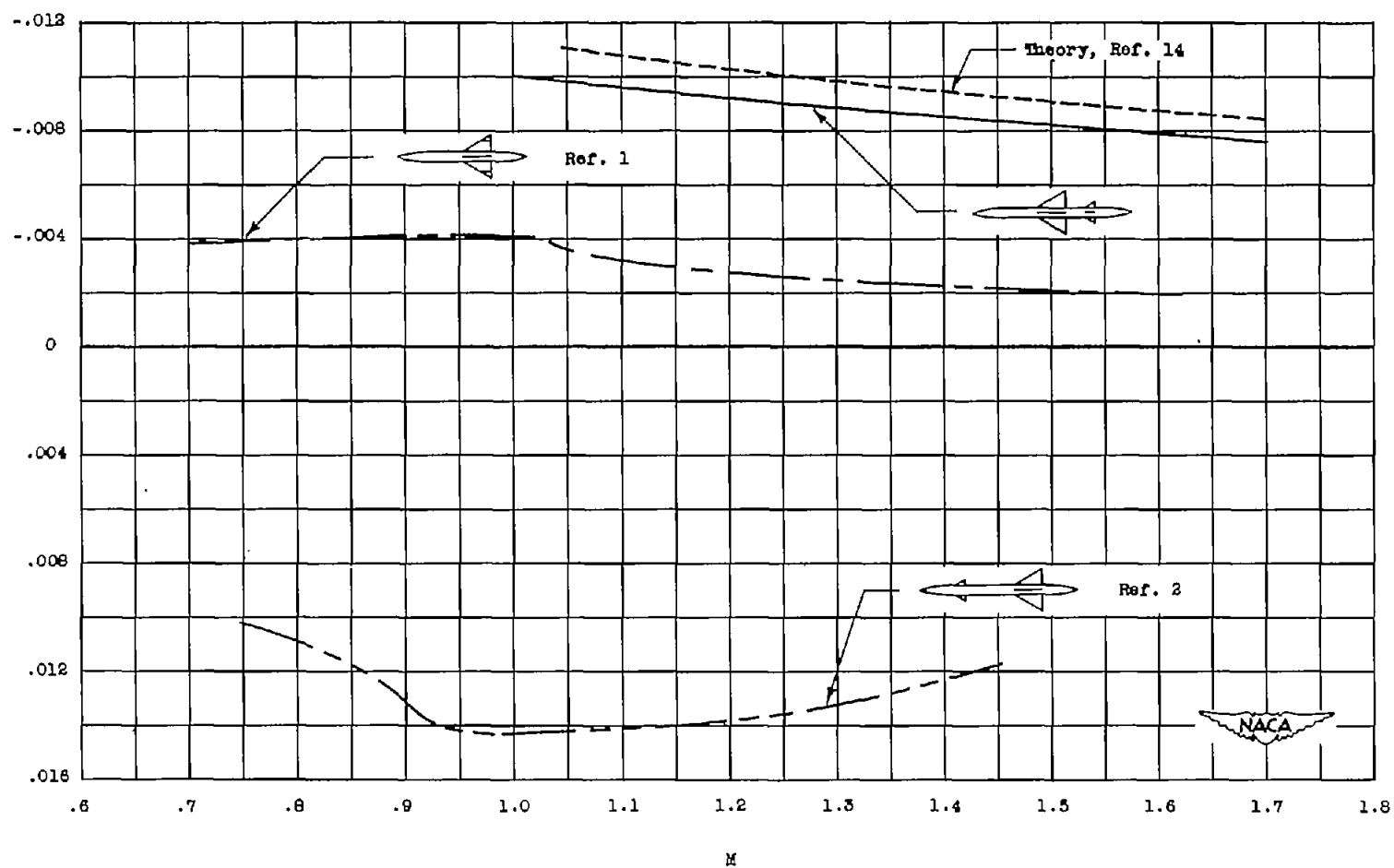
Figure 18.- Tail pitching effectiveness.
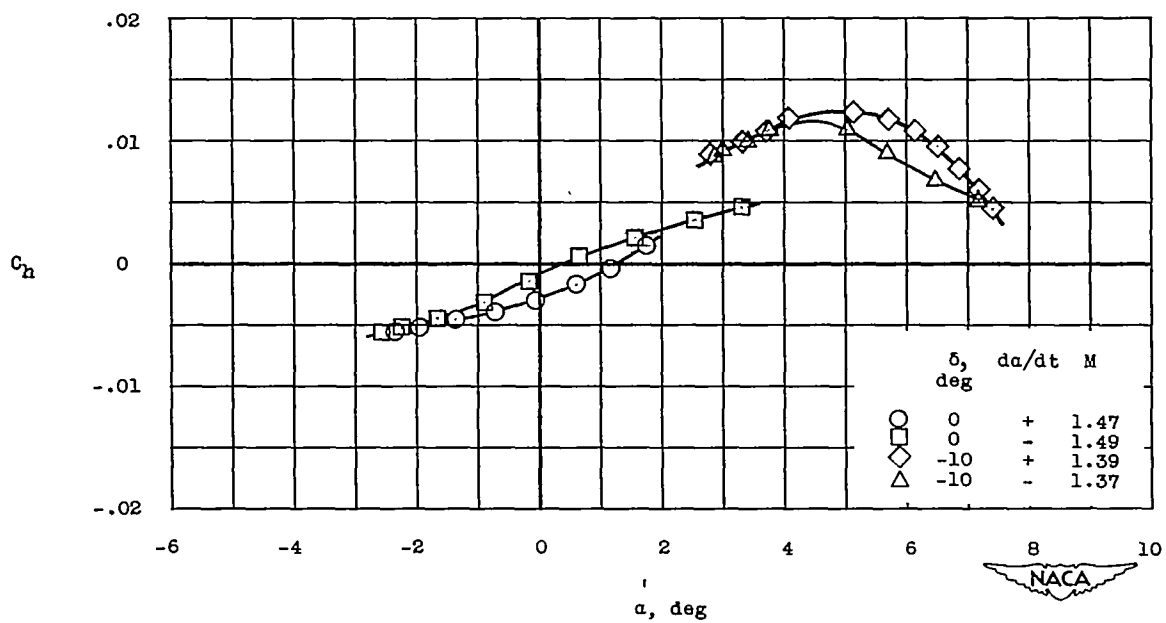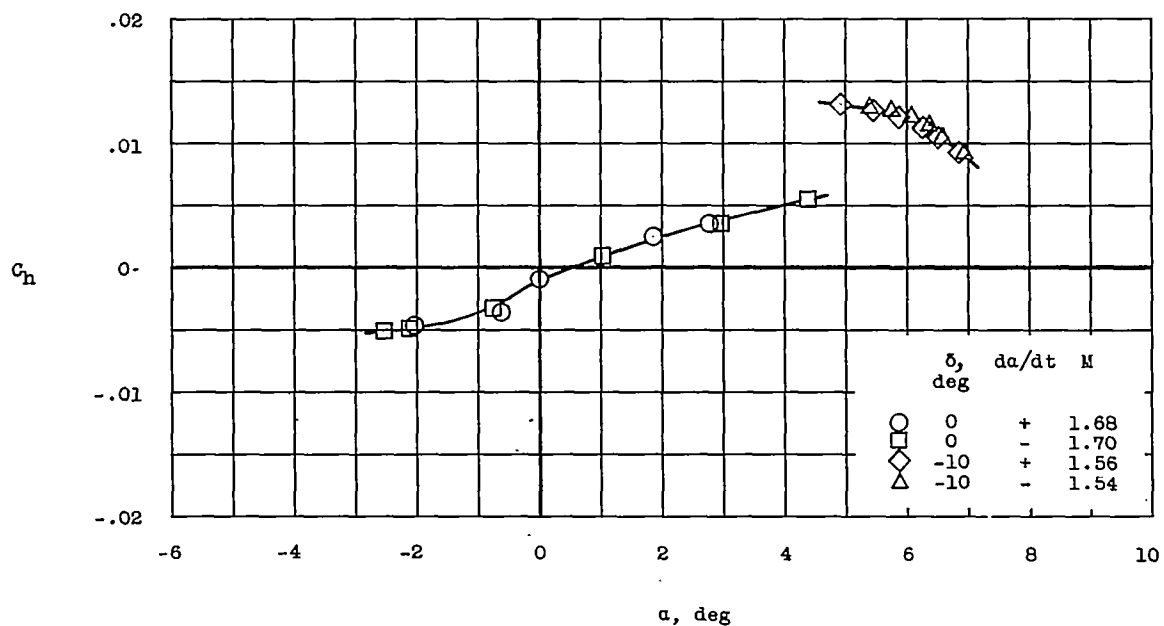
Figure 19.- Variation of control-surface hinge-moment coefficient with angle of attack.
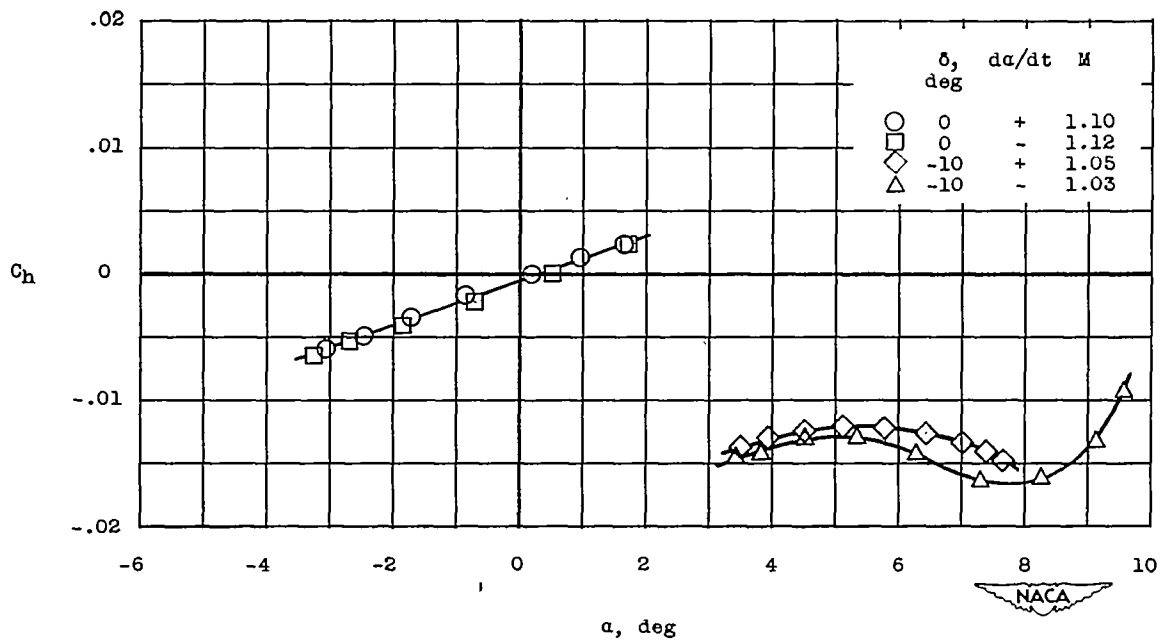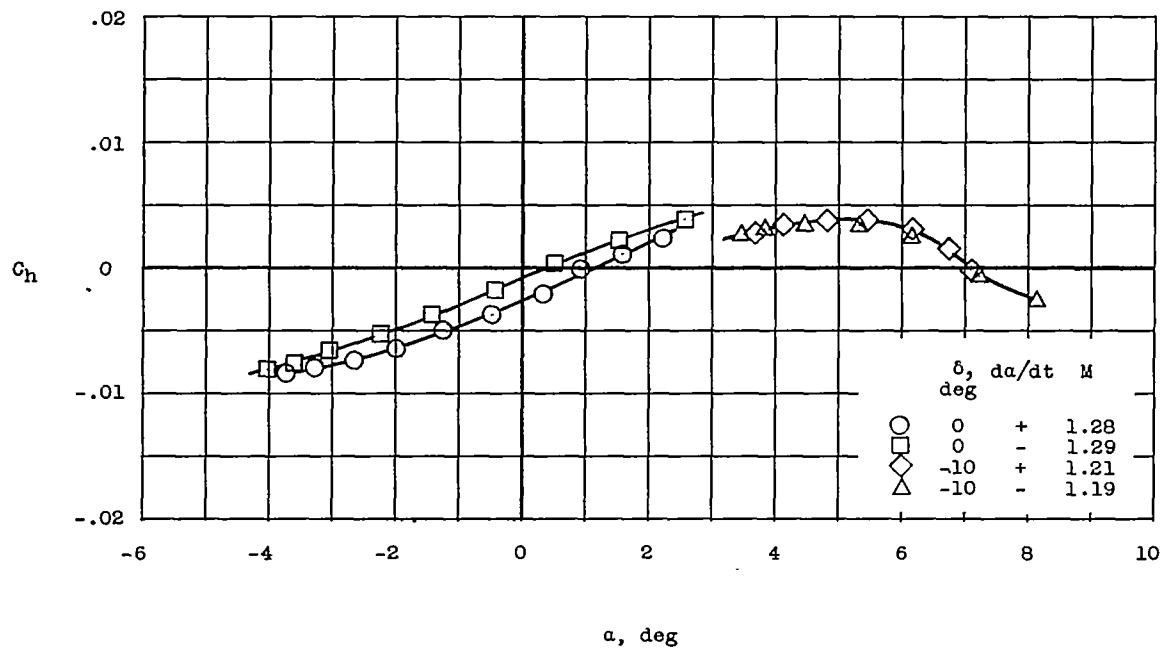
Figure 19.- Continued.
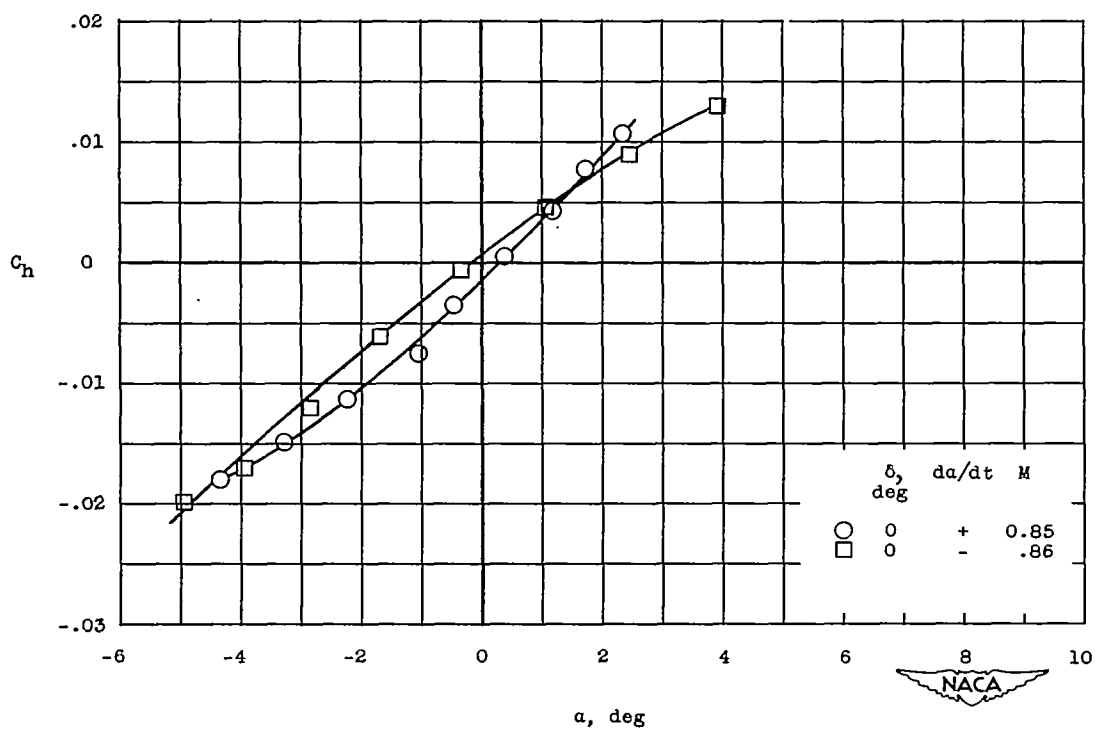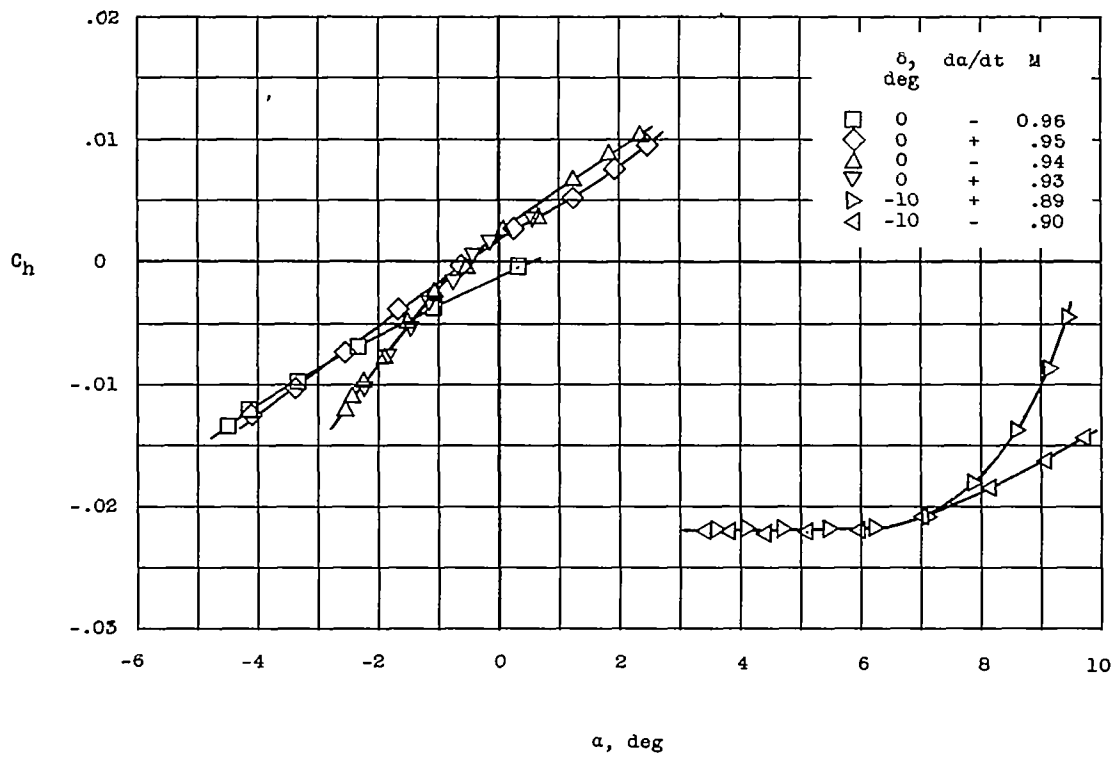
Figure 19.- Concluded.
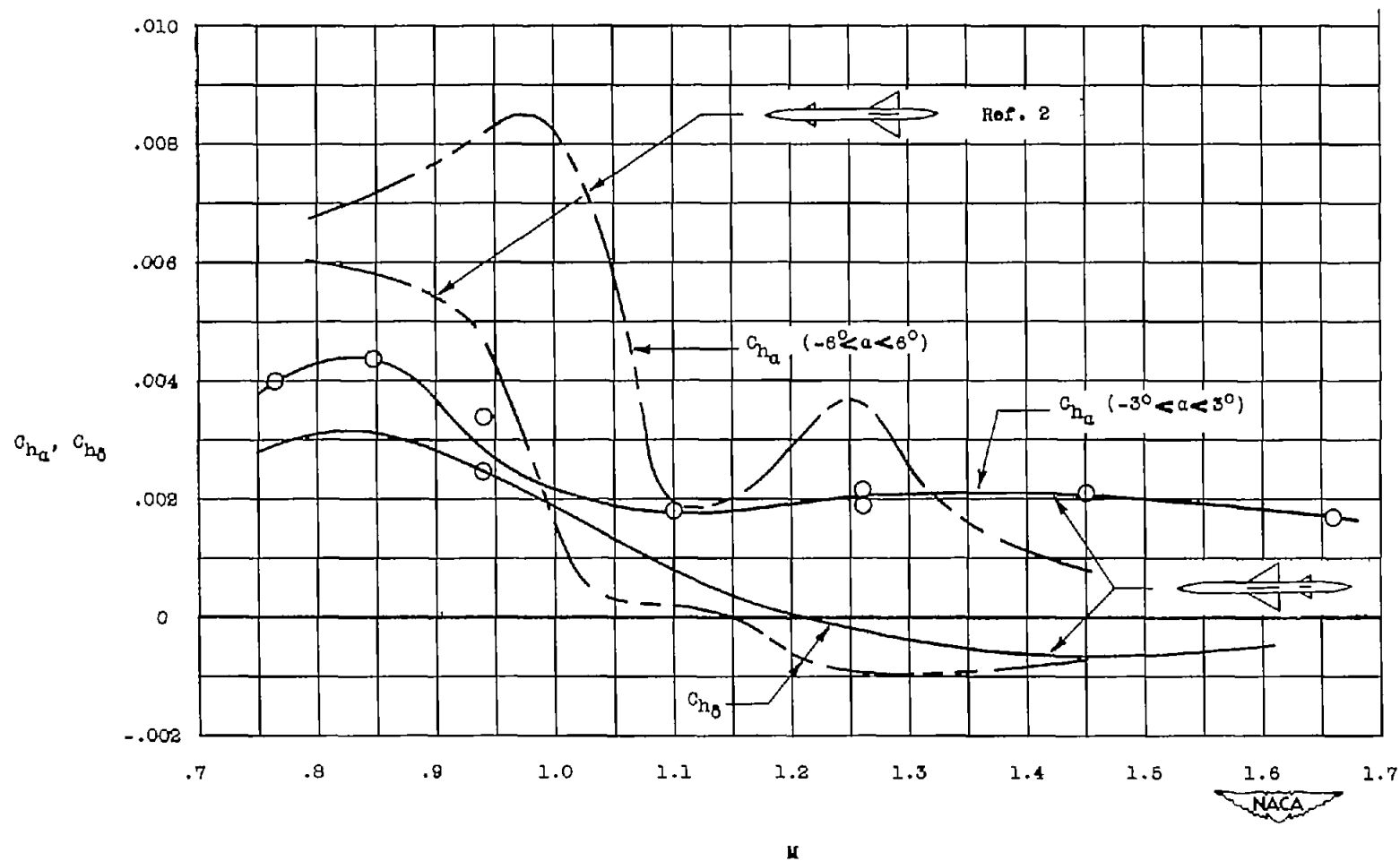
Figure 20.- Variation of hinge-moment-coefficient derivatives with Mach number.
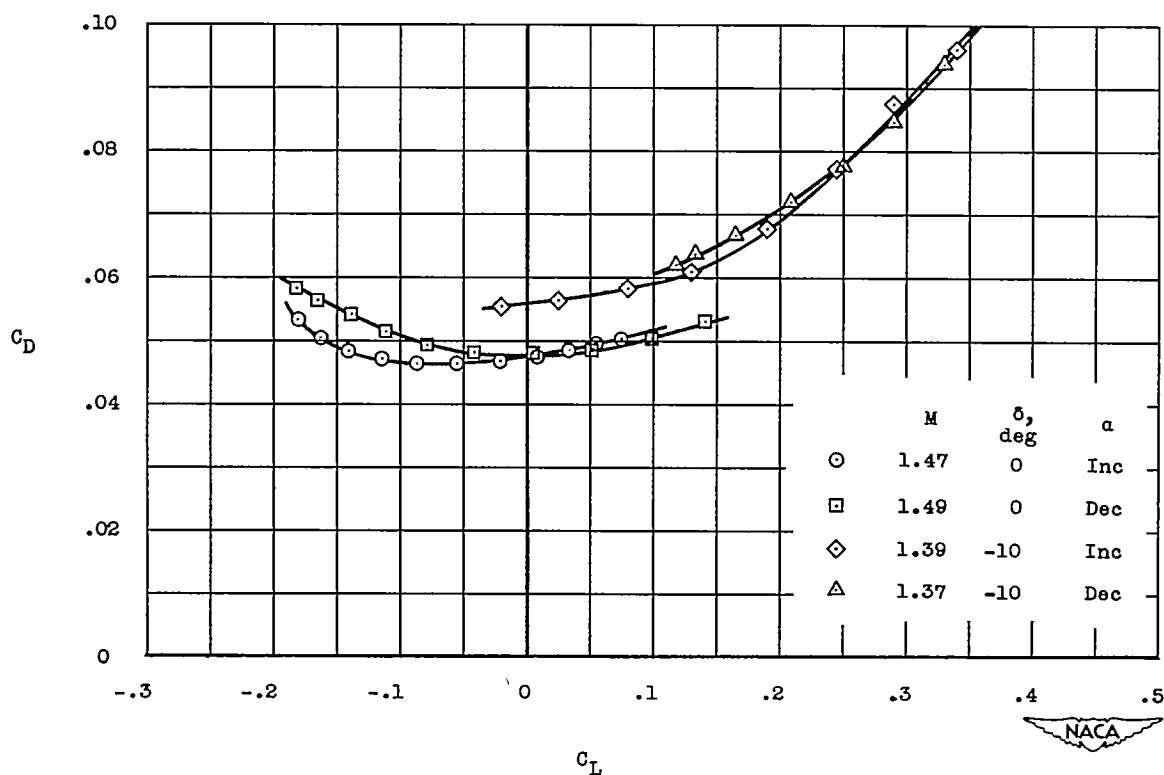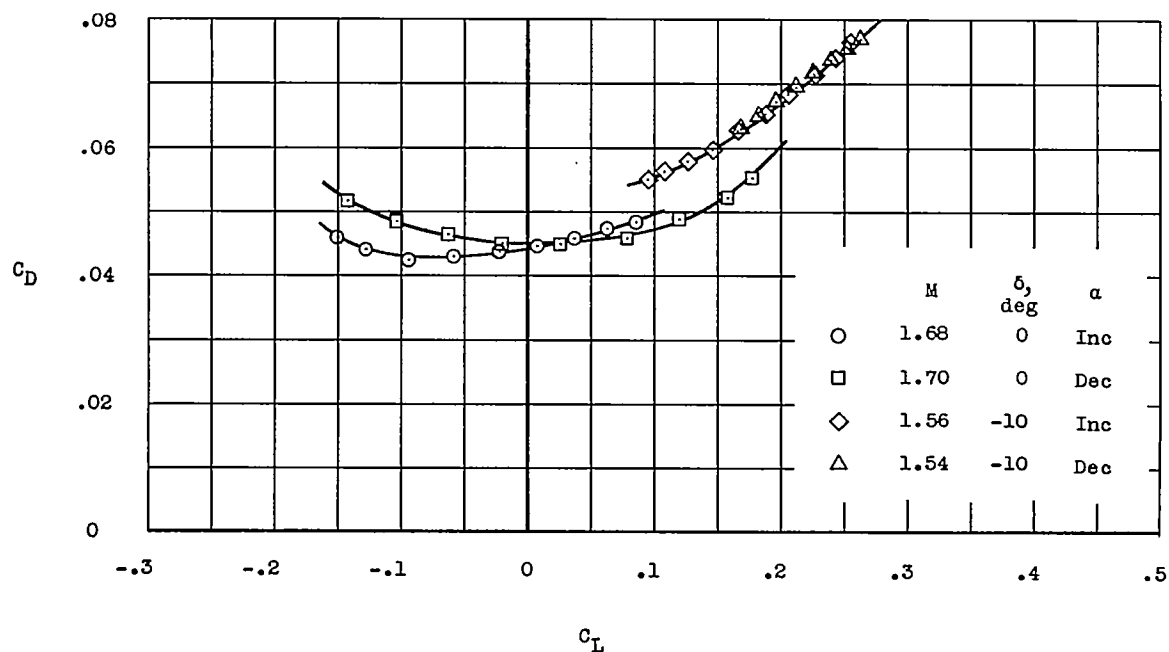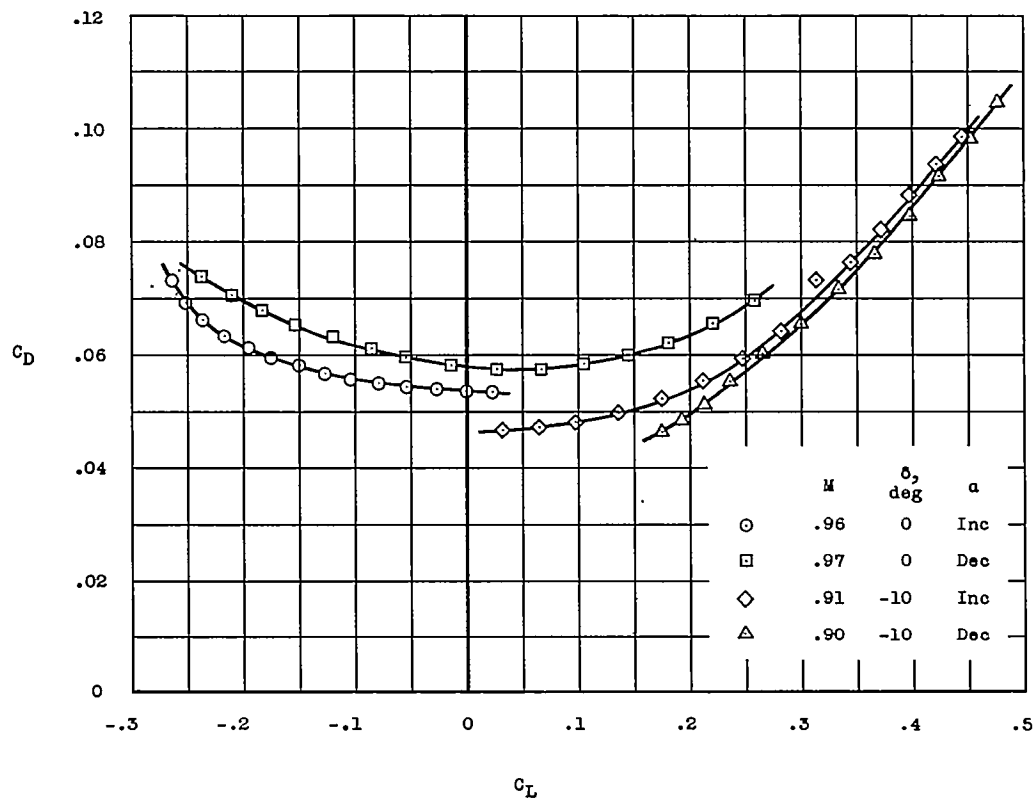
Figure 21.- Lift-drag polars.
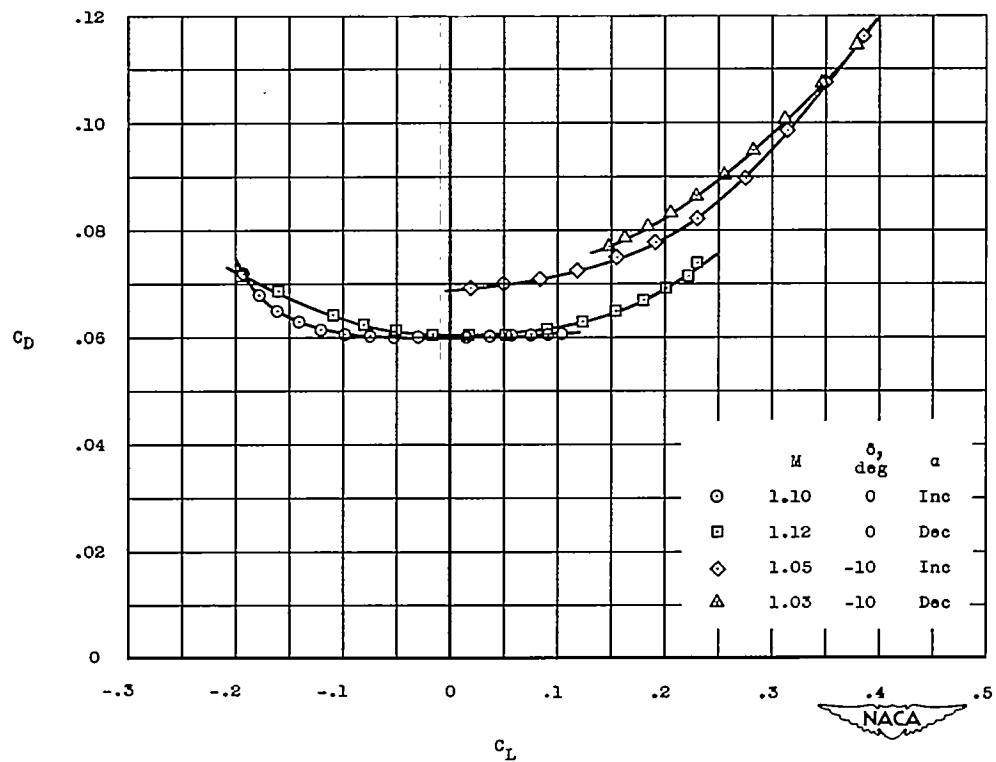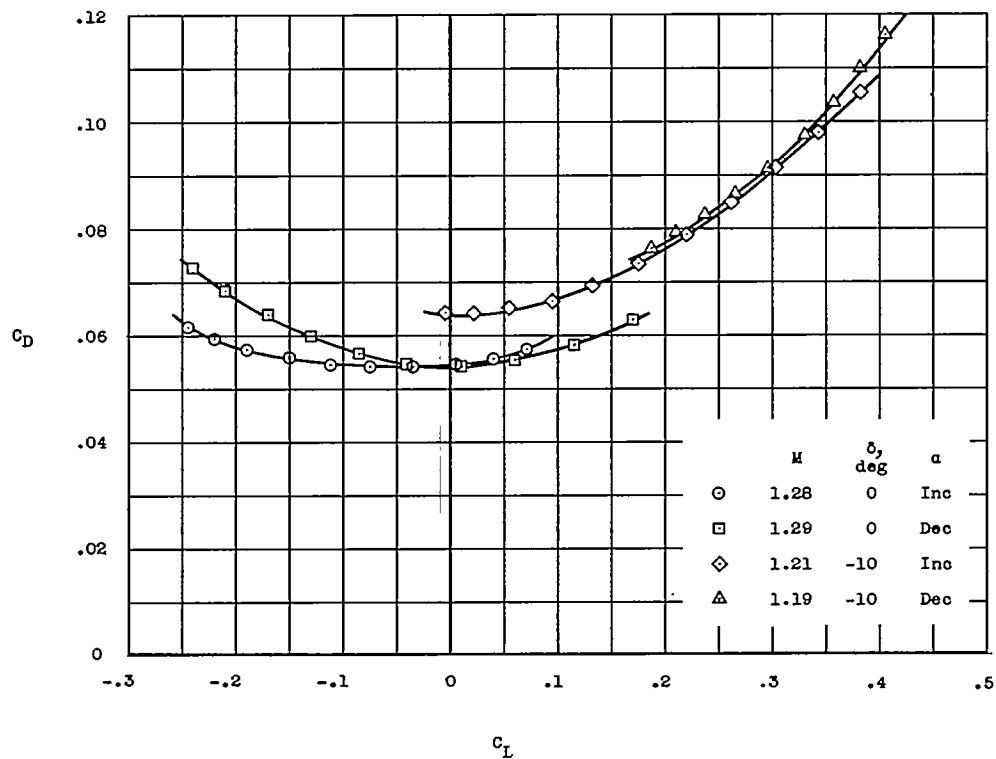
Figure 21.- Continued.
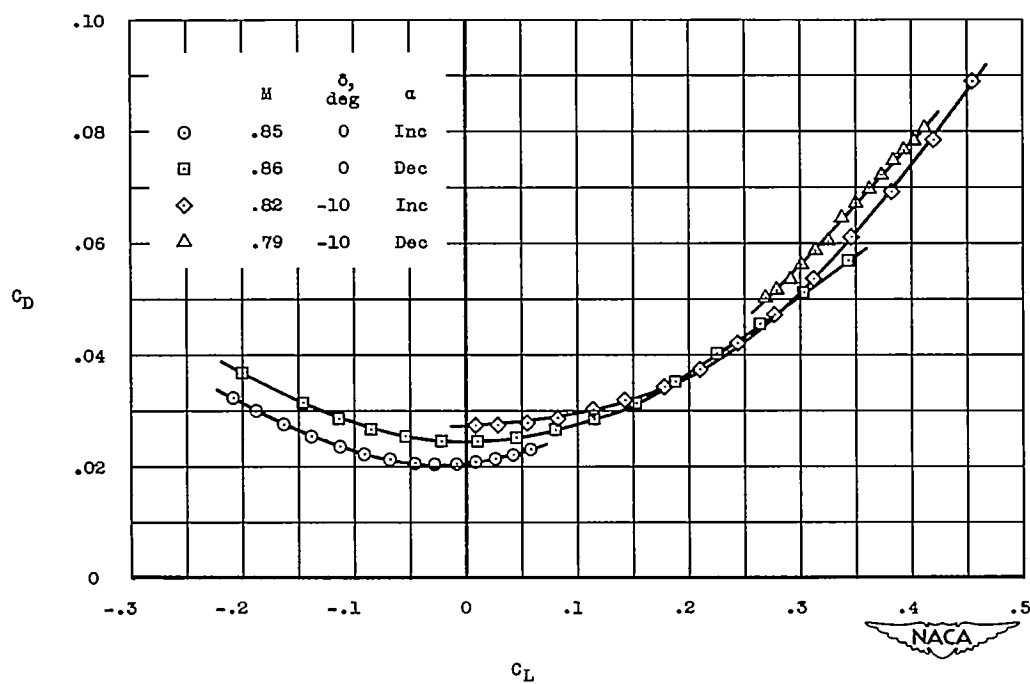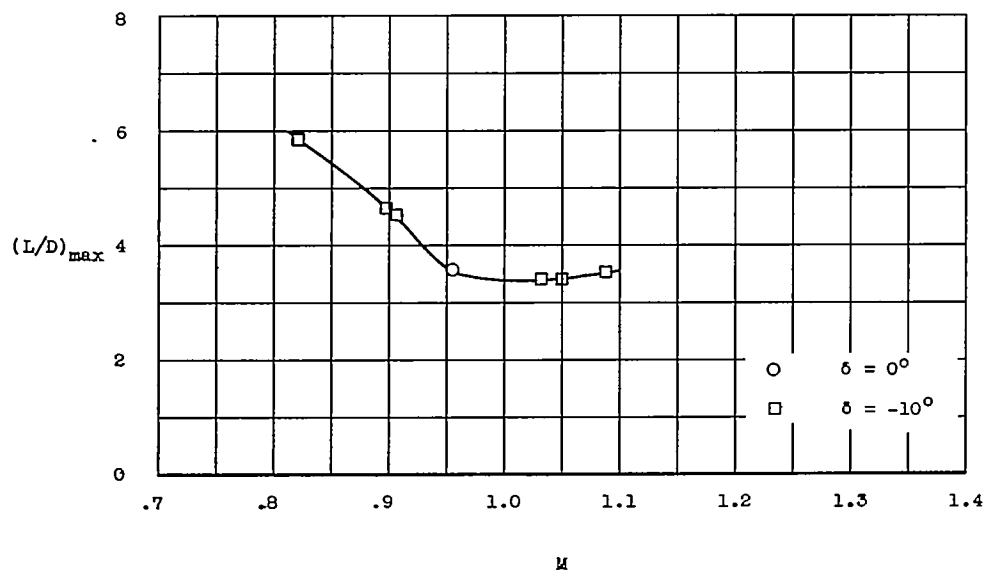
Figure 21.- Concluded.

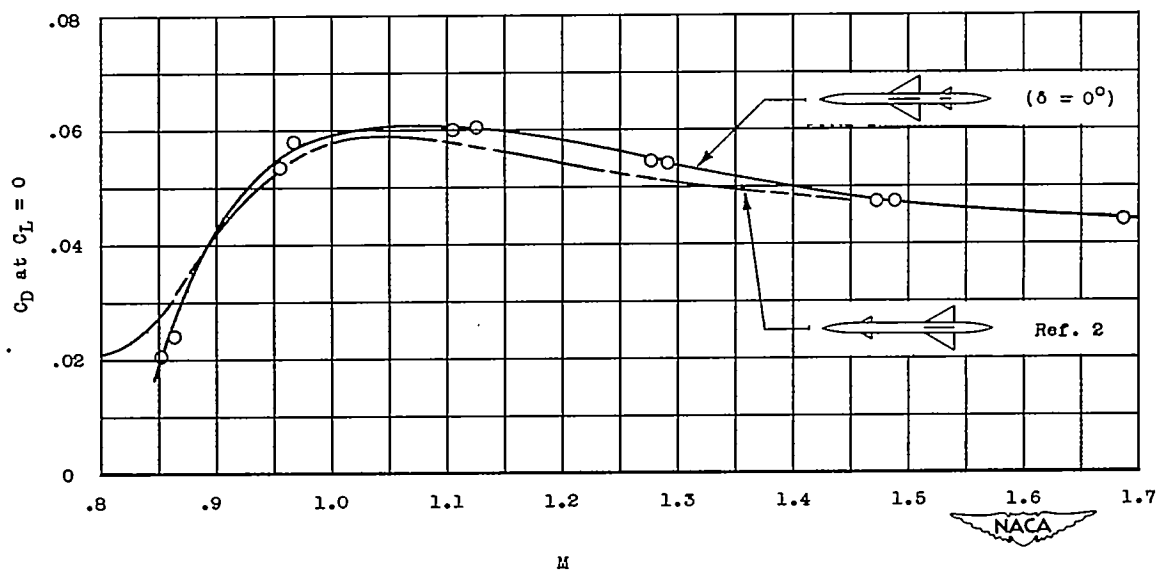Figure 22.- Variation of maximum lift-drag ratio with Mach number.

Figure 23.- Variation of drag coefficient at zero lift with Mach number.